iScience

CellPress
OPEN ACCESS

Article

SHP2 mutations promote glycolysis and inhibit apoptosis via PKM2/hnRNPK signaling in colorectal cancer

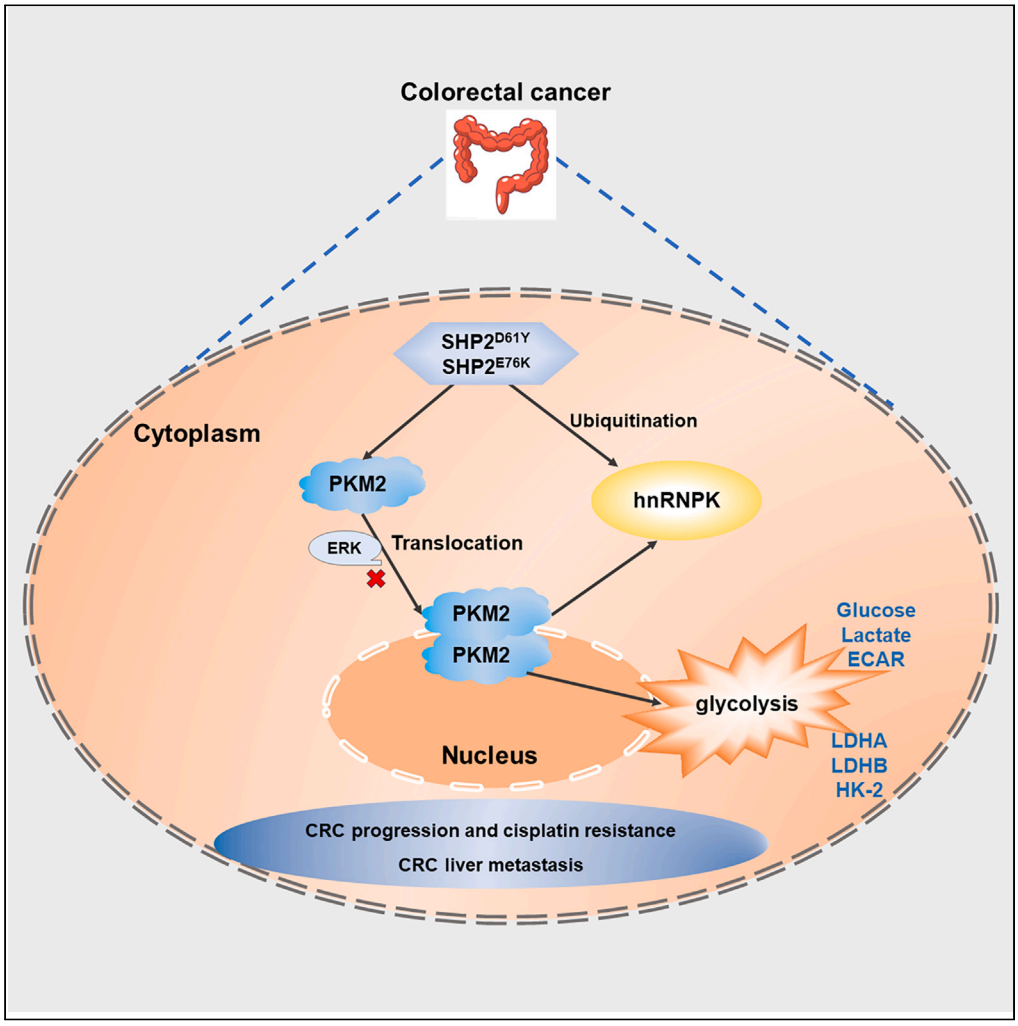

Bo Zhou, Zhuoyang Fan, Guodong He, ..., Lechi Ye, Jianmin Xu, Rong Liu

yljwenzhou@126.com (L.Y.)
xujmin@aliyun.com (J.X.)
liu.rong@zs-hospital.sh.cn (R.L.)

Highlights

SHP2^{D61Y} and SHP2^{E76K} promote CRC cell migration/invasion and inhibit apoptosis

SHP2^{D61Y} and SHP2^{E76K} promote tumor growth and liver metastasis of CRC *in vivo*

SHP2^{D61Y} and SHP2^{E76K} promote CRC glycolysis through PKM2 nuclear translocation

PKM2 increases CRC cell migration/invasion by regulating hnRNPK ubiquitination

Zhou et al., iScience 27, 110462
August 16, 2024
https://doi.org/10.1016/j.isci.2024.110462

iScience

CellPress
OPEN ACCESS

Article

SHP2 mutations promote glycolysis and inhibit apoptosis via PKM2/hnRNPK signaling in colorectal cancer

Bo Zhou,[1,2,3,7] Zhuoyang Fan,[1,2,3,7] Guodong He,[4,5,7] Wei Zhang,[1,2,3] Guowei Yang,[1,2,3] Lechi Ye,[6,*] Jianmin Xu,[4,5,*] and Rong Liu[1,2,3,8,*]

SUMMARY

Colorectal cancer (CRC) is one of the most common gastrointestinal tumors. Src homology-2 domain-containing protein tyrosine phosphatase-2 (SHP2) mutations occur in human solid tumors, including CRC. However, the function and underlying mechanism in CRC have not been well characterized. We demonstrated that the $SHP2^{D61Y}$ and $SHP2^{E76K}$ mutations occurred in CRC tissues, and these mutations promoted CRC cell proliferation, migration/invasion, and reduced CDDP-induced cell apoptosis *in vitro* and *in vivo*. Mechanistically, $SHP2^{D61Y}$ and $SHP2^{E76K}$ promote glycolysis by accelerating pyruvate kinase M2 (PKM2) nuclear translocation through mechanism beyond ERK activation. PKM2-IN-1 attenuates PKM2-dependent glycolysis and reduce glucose uptake, lactate production, and ATP levels promoted by $SHP2D^{61Y}$ and $SHP2^{E76K}$ in CRC cells. Furthermore, PKM2 upregulates heterogeneous nuclear ribonucleoprotein K (hnRNPK) expression and increases CRC cell proliferation and migration/invasion via regulating hnRNPK ubiquitination. These findings provide evidence that $SHP2^{D61Y}$ and $SHP2^{E76K}$ regulate CDDP-induced apoptosis, glucose metabolism, and CRC migration/invasion through PKM2 nuclear translocation and PKM2/hnRNPK signaling.

INTRODUCTION

Colorectal cancer (CRC) is one of the most common gastrointestinal tumors worldwide and has a high risk of metastases.[1,2] The epidemiology of CRC varies between regions and involves several factors including genetic susceptibility and mutations, which can also influence prognosis and response to treatment.[3] However, a profile of mutations involved in the progression and metastasis of CRC is beginning to emerge.[4,5] Several molecular pathways including those that promote glycolysis are associated with the progression of CRC.[6,7]

The upregulation of pyruvate kinase M2 (PKM2) increases glucose consumption and cellular ATP production to promote glycolysis and the progression of CRC.[6] PKM2 is generated through the alternative splicing of PKM and its activation and nuclear relocation contribute to aerobic glycolysis in the tumor environment.[8,9] The nuclear relocation of PKM2 leads to the activation of glycolysis-related genes through several interactions that are thought to involve the Wnt/β-catenin pathway, epidermal growth factor receptor (EGFR), and heterogeneous nuclear ribonucleoprotein K (hnRNPK).[10–12] The inhibition of PKM2-mediated glycolysis can prevent drug resistance in CRC.[13] Moreover, several studies have found that the downregulation of PKM2 can inhibit the growth and metastasis of CRC.[14]

Src homology-2 domain-containing protein tyrosine phosphatase-2 (SHP2) is associated with gain-of-function mutations in solid tumors, including CRC.[15,16] E76K and D61Y are somatic mutations in SHP2 that are known to be associated with CRC.[17] However, the function and underlying mechanism of these mutations in the progression of CRC are not well characterized. A previous study found that ERK1/2 phosphorylates PKM2 at Ser37 and recruits importin α5 to promote PKM2 translocation into the nucleus upon EGFR activation.[18] Therefore, in the present study, we determined whether SHP2 is involved in the phosphorylation and nuclear translocation of PKM2 and the role played by ERK phosphorylation.

The aim of this study was mainly to ascertain whether $SHP2^{D61Y}$ and $SHP2^{E76K}$ mutations could alter the function of SHP2 in CRC. We measured the interactions of $SHP2^{WT}$, $SHP2^{D61Y}$, and $SHP2^{E76K}$ with PKM2 and hnRNPK in CRC tissues and cell lines and determined whether

[1]Department of Interventional Radiology, Zhongshan Hospital Fudan University, Shanghai 200032, China
[2]National Clinical Research Center for Interventional Medicine, Shanghai 200032, China
[3]Shanghai Institute of Medical Imaging, Shanghai 200032, China
[4]Department of Colorectal Surgery, Zhongshan Hospital Fudan University, Shanghai 200032, China
[5]Shanghai Engineering Research Center of Colorectal Cancer Minimally Invasive Technology, Shanghai 200032, China
[6]Department of Colorectal and Anal Surgery, The First Affiliated Hospital of Wenzhou Medical University, Wenzhou 325000, China
[7]These authors contributed equally
[8]Lead contact
*Correspondence: yljwenzhou@126.com (L.Y.), xujmin@aliyun.com (J.X.), liu.rong@zs-hospital.sh.cn (R.L.)
https://doi.org/10.1016/j.isci.2024.110462

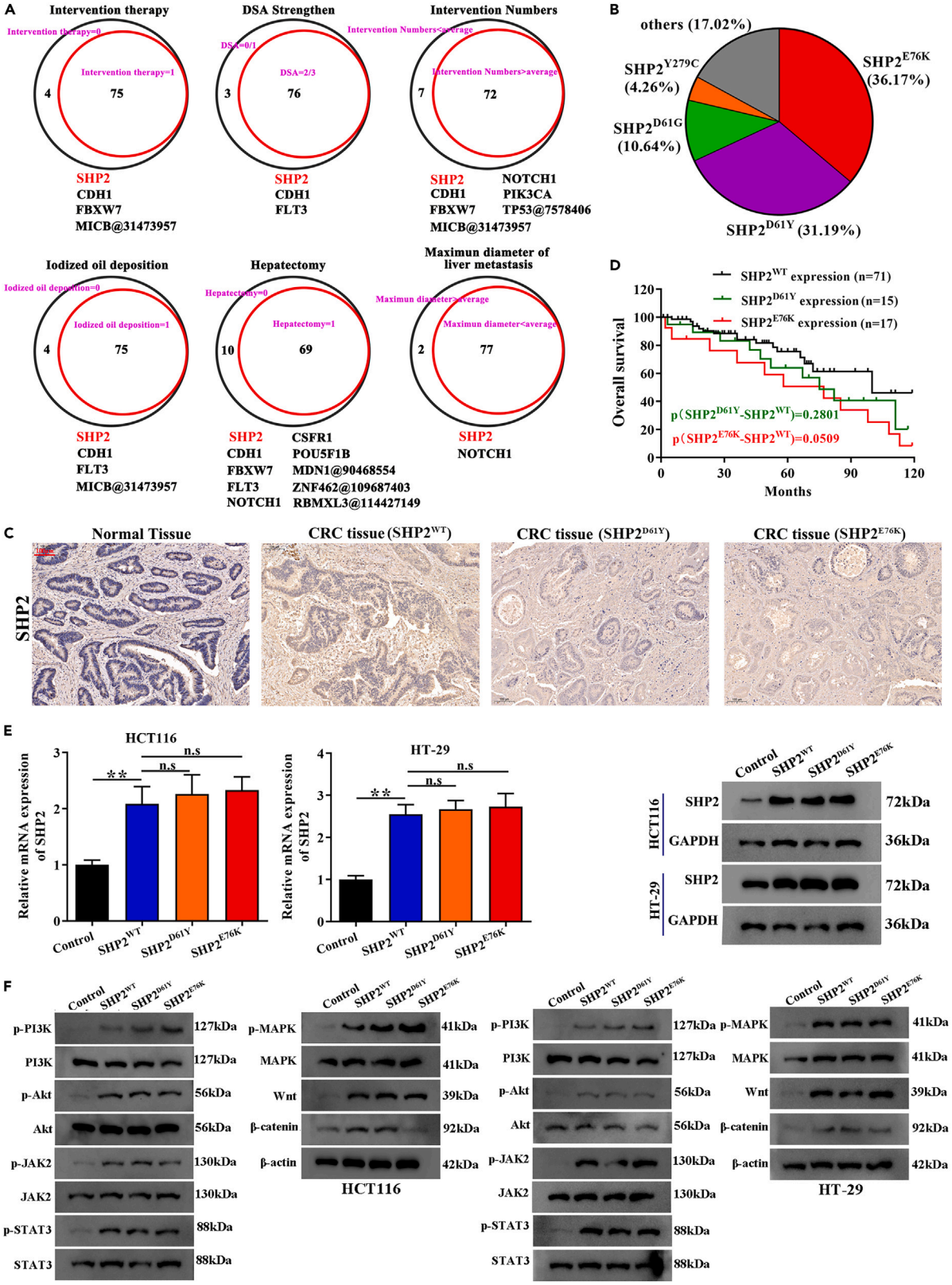
A
Intervention therapy
Intervention therapy=0
Intervention therapy=1
4
75
SHP2
CDH1
FBXW7
MICB@31473957
DSA Strengthen
DSA=0/1
DSA=2/3
3
76
SHP2
CDH1
FLT3
Intervention Numbers
Intervention Numbers<average
Intervention Numbers>average
7
72
SHP2
CDH1
FBXW7
MICB@31473957
NOTCH1
PIK3CA
TP53@7578406
Iodized oil deposition
Iodized oil deposition=0
Iodized oil deposition=1
4
75
SHP2
CDH1
FLT3
MICB@31473957
Hepatectomy
Hepatectomy=0
Hepatectomy=1
10
69
SHP2
CDH1
FBXW7
FLT3
NOTCH1
CSFR1
POU5F1B
MDN1@90468554
ZNF462@109687403
RBMXL3@114427149
Maximun diameter of liver metastasis
Maximun diameter<average
2
77
SHP2
NOTCH1
B
others (17.02%)
SHP2E76K (36.17%)
SHP2Y279C (4.26%)
SHP2D61G (10.64%)
SHP2D61Y (31.19%)
D
SHP2WT expression (n=71)
SHP2D61Y expression (n=15)
SHP2E76K expression (n=17)
Overall survival
p(SHP2D61Y-SHP2WT)=0.2801
p(SHP2E76K-SHP2WT)=0.0509
Months
C
Normal Tissue
CRC tissue (SHP2WT)
CRC tissue (SHP2D61Y)
CRC tissue (SHP2E76K)
SHP2
E
HCT116
HT-29
Relative mRNA expression of SHP2
n.s
**
Control
SHP2WT
SHP2D61Y
SHP2E76K
HCT116
HT-29
SHP2
GAPDH
72kDa
36kDa
F
p-PI3K
PI3K
p-Akt
Akt
p-JAK2
JAK2
p-STAT3
STAT3
p-MAPK
MAPK
Wnt
β-catenin
β-actin
127kDa
56kDa
130kDa
88kDa
41kDa
39kDa
92kDa
42kDa
HCT116
HT-29

Figure 1. SHP2 mutations are highly expressed in colorectal cancer (CRC)

(A) Mutated gene analysis from patients with a poor response to several therapy (interventional therapy, DSA strengthen, intervention numbers, iodized oil deposition, hepatectomy, maximum diameter of liver metastasis) in patients with colorectal cancer (n = 47) is shown.

(B) The occurrence of SHP2 mutation site (E76K, D61Y, D61G, Y279C, and others) in CRC were shown in distribution diagram.

(C) SHP2 protein expression in normal tissues and CRC tissues ($SHP2^{WT}$, $SHP2^{D61Y}$ and $SHP2^{E76K}$) was determined by immunohistochemistry.

(D) Kaplan-Meier curves for the overall survival of CRC patients according to wild type ($SHP2^{WT}$) or mutated ($SHP2^{D61Y}$, $SHP2^{E76K}$) SHP2.

(E) The mRNA and protein expression levels of SHP2 in HCT116 and HT-29 cells transfected with Control, $SHP2^{WT}$, $SHP2^{D61Y}$, and $SHP2^{E76K}$ were measured by qRT-PCR and western blotting (n = 3).

(F) The protein expression levels of p-PI3K, total PI3K, p-Akt, total Akt, p-JAK2, total JAK2, p-STAT3, total STAT3, p-mitogen-activated protein kinase (MAPK), total MAPK, Wnt, and β-catenin in HCT116 and HT-29 cells transfected with Control, $SHP2^{WT}$, $SHP2^{D61Y}$, and $SHP2^{E76K}$ were detected by western blotting (n = 3).

*$p < 0.05$, **$p < 0.01$, and ***$p < 0.001$.

they could influence the proliferation, migration/invasion, and glycolysis of CRC cells with and without cisplatin (CDDP). Furthermore, we investigated whether the ubiquitination of hnRNPK may in turn be regulated by PKM2, given that hnRNPK and its degradation are associated with the progression and metastasis of several cancers, including CRC.[12,19,20] Our findings provide evidence that the $SHP2^{D61Y}$ and $SHP2^{E76K}$ regulate CDDP-induced apoptosis, glucose metabolism, migration/invasion, and hepatic metastasis in CRC through PKM2 nuclear translocation and PKM2/hnRNPK signaling. Mechanistically, we found that $SHP2^{D61Y}$ and $SHP2^{E76K}$ accelerate PKM2 nuclear translocation through mechanisms beyond ERK activation, suggesting the involvement of additional regulatory pathways. This study supports evidence that SHP2, PKM2, or associated pathways could be therapeutic targets in the treatment of CRC.

RESULTS

SHP2 mutations are highly expressed in CRC

We collected data from 47 patients with liver metastases derived from CRC, each of whom had genetic variant information and clinical information. We analyzed patient response and variant information after intervention to search for variants that were prevalent in patients with poor interventional efficacy (Figure 1A). In Figure 1A, compared with interventional therapy once, there were 4 unique genes in interventional therapy 0 times; compared with DSA strengthen 2/3 times, there were 3 unique genes in DSA strengthen none or once; compared with interventional numbers over the average, there were 7 unique genes in interventional numbers below the average; compared with iodized oil deposition once, there were 4 unique genes in iodized oil deposition 0 times; compared with hepatectomy once, there were 10 unique genes in hepatectomy 0 times; compared with maximum diameter of liver metastasis below average, there were 2 unique genes in maximum diameter of liver metastasis over average. In all therapy, the SHP2 is the only common mutant genes. The SHP2 gene accounts for the majority of differential expression found in a disease-specific array for CRC. In an analysis of SHP2 mutations in CRC, E76K, and D61Y occurred the most frequently at expression levels of 36.17% and 31.19%, respectively, with D61G, Y279C, and others comprising less than 20% of the expression (Figure 1B). Immunohistochemistry confirmed the high levels of SHP2 protein expression in CRC tissues compared to normal tissues (Figure 1C) and we used Kaplan-Meier curves to determine the importance of the mutations in the overall survival (OS) of patients with CRC (Figure 1D). However, the OS between $SHP2^{WT}$ and SHP2 mutation ($SHP2^{D61Y}$ and $SHP2^{E76K)}$ has no statistically significant difference. Subsequently, the association between SHP2-WT and SHP2 mutation and clinicopathological characteristics of patients with CRC are presented in Table S1. Statistical analyses of $SHP2^{WT}$ and SHP2 mutated expression and CRC clinical pathological features revealed that the $SHP2^{D61Y}$ and $SHP2^{E76K}$ group had much more advanced T, N, M, and TNM stages than the $SHP2^{WT}$ group. To determine the expression level of each mutation, HCT116 and HT-29 cells were transfected with $SHP2^{WT}$, $SHP2^{D61Y}$, and $SHP2^{E76K}$. Subsequent quantitative real-time PCR (qRT-PCR) and western blotting indicated that the expression of between $SHP2^{E76K}$, $SHP2^{D61Y}$, and $SHP2^{WT}$ has no significant difference in both cell lines (Figure 1E). Due to the HCT116 cells contain β-catenin and KRAS mutations, and HT29 cells contain APC and BRAF mutations, these mutations may affect the expression of Janus kinase 2/signal transducer and activator of transcription 3(JAK2/STAT3), PI3K/protein kinase B (Akt), and Wnt/β-catenin signaling pathways. So, we have examined the protein expression levels of SHP2 on JAK2/STAT3, PI3K/Akt, and Wnt/β-catenin signaling pathways, the results are shown in Figure 1F. The results indicated that the expression levels between $SHP2^{WT}$ and SHP2 mutation ($SHP2^{D61Y}$ and $SHP2^{E76K}$) have no significant difference on JAK2/STAT3, PI3K/Akt, and Wnt/β-catenin signaling pathways. These also demonstrated that SHP2 mutation in CRC cell lines here did not affect the prooncogenic potential of the SHP2 mutations (Figure 1F). These results demonstrate the significance of mutations on the expression of SHP2 in CRC. $SHP2^{D61Y}$ and $SHP2^{E76K}$ are not only expressed at higher levels in CRC cells but they are also associated with a lower OS.

$SHP2^{D61Y}$ and $SHP2^{E76K}$ promote proliferation, migration, and invasion in CRC cells

Cell proliferation and viability in HCT116 and HT-29 cells expressing $SHP2^{WT}$, $SHP2^{D61Y}$, and $SHP2^{E76K}$ were further evaluated with EdU (5-ethynyl-2′-deoxyuridine) and colony formation assays. Cell proliferation and viability were higher in cells expressing $SHP2^{D61Y}$ and $SHP2^{E76K}$ than in those expressing $SHP2^{WT}$ (Figures 2A and 2B). Apoptosis was also assessed in HCT116 and HT-29 cells expressing $SHP2^{D61Y}$ and $SHP2^{E76K}$ using flow cytometry. The rate of apoptosis was significantly lower in cells expressing SHP2 with D61Y or E76K mutations (Figure 2C). Migration and invasion capabilities of HCT116 and HT-29 cells expressing $SH2^{WT}$, $SHP2^{D61Y}$, and $SHP2^{E76K}$ were evaluated with Matrigel-coated transwell assays. Invasion and migration were significantly increased in cells expressing the two SHP2 variants (Figure 2D), and CRC cells harboring $SHP2^{E76K}$ showed the most aggressive invasion and migration.

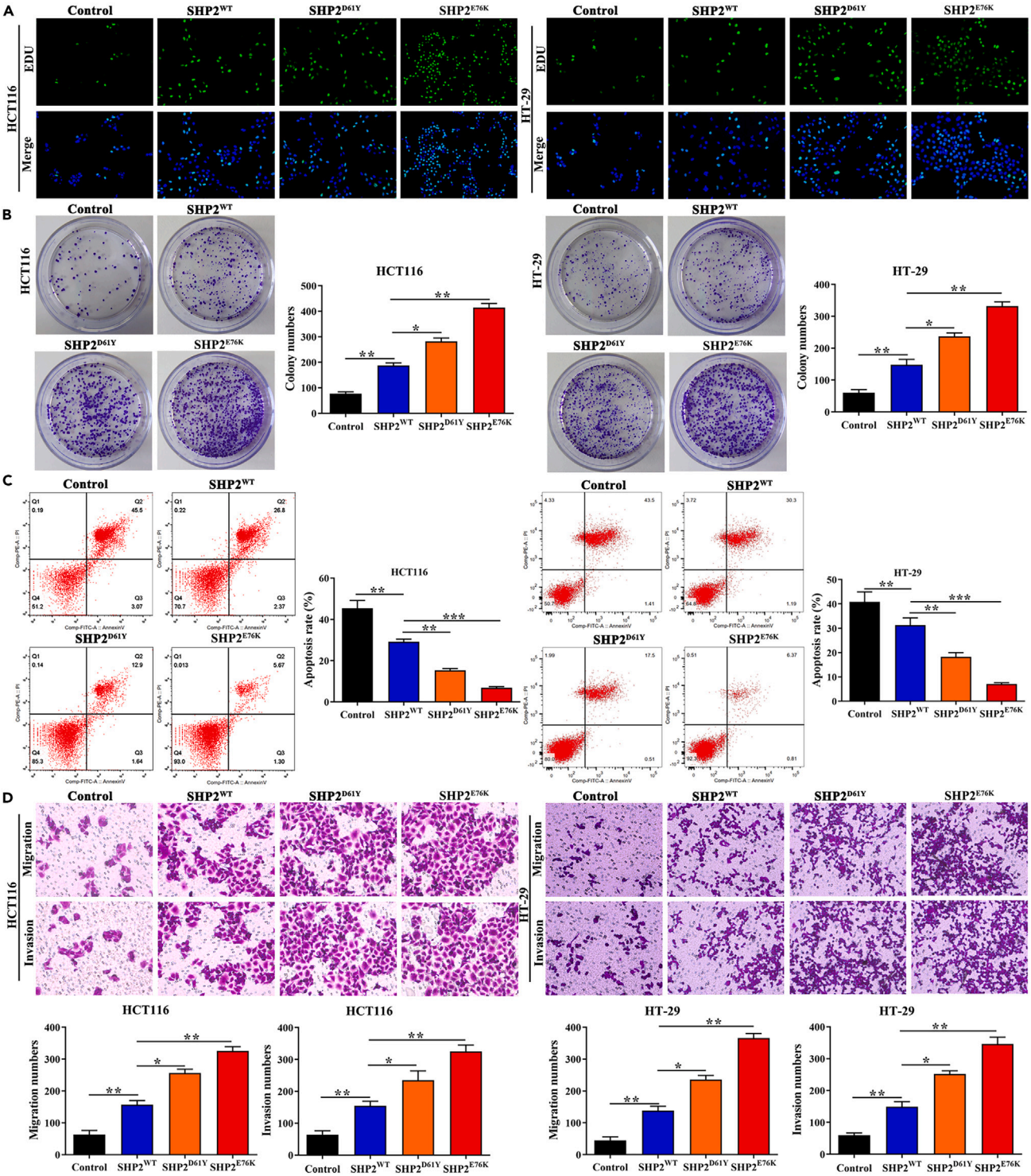

Figure 2. SHP2^{D61Y} and SHP2^{E76K} promote colorectal cancer (CRC) cell proliferation and migration/invasion

(A) Cell proliferation in HCT116 and HT-29 cells transfected with control, SHP2^{WT}, SHP2^{D61Y}, and SHP2^{E76K} were evaluated via the determination of cell viability by using EdU assays.

(B) The colony formation capability in HCT116 and HT-29 cells transfected with Control, SHP2^{WT}, SHP2^{D61Y} and SHP2^{E76K} were determined by colony formation assay.

(C) Flow cytometry assays were performed to assess the apoptosis rate in HCT116 and HT-29 cells transfected with control, SHP2^{WT}, SHP2^{D61Y}, and SHP2^{E76K}.

(D) Migration/invasion capabilities of HCT116 and HT-29 cells transfected with Control, SHP2^{WT}, SHP2^{D61Y}, and SHP2^{E76K} were evaluated with Matrigel-coated transwell assays. *$p < 0.05$, **$p < 0.01$, and ***$p < 0.001$.

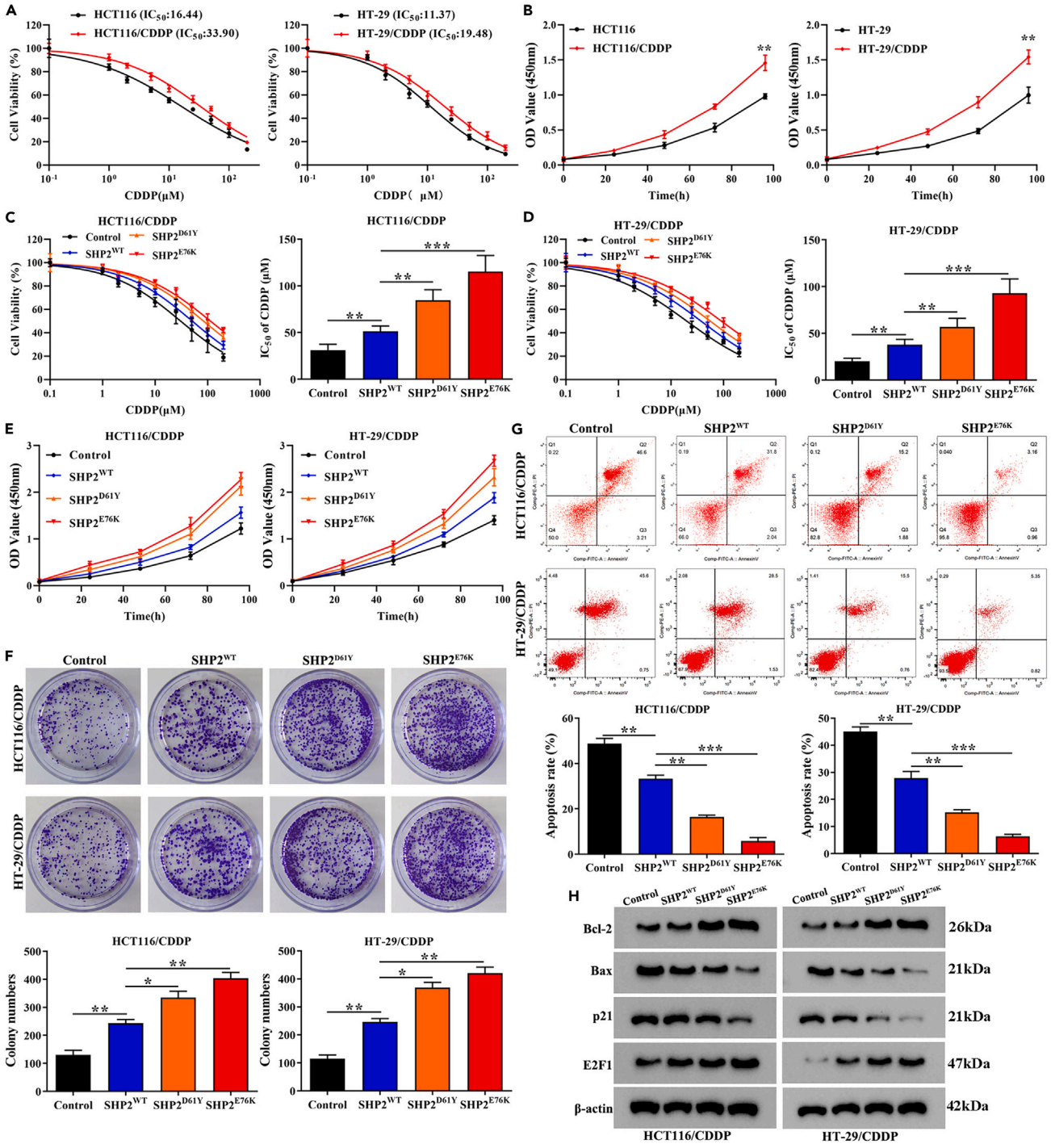

Figure 3. SHP2^{D61Y} and SHP2^{E76K} inhibit colorectal cancer (CRC) cell apoptosis and increase cisplatin (CDDP) resistance

(A) CCK-8 assays were used to detect cell viability and IC_{50} values in CRC cancer cells (HCT116 and HT-29) and CDDP-resistant CRC cancer cells (HCT116/CDDP and HT-29/CDDP) and quantified by Graph Prism 8.0.

(B) Cell viabilities in cancer cells (HCT116 and HT-29) and CDDP-resistant cancer cells (HCT116/CDDP and HT-29/CDDP) were determined at different times (24, 48, 72, 96, and 120 h).

(C and D) Cell viabilities and IC_{50} values were detected in HCT116/CDDP and HT-29/CDDP cells, which were transfected with control, SHP2^{WT}, SHP2^{D61Y}, and SHP2^{E76K}.

(E) Cell viabilities were detected at different times (24, 48, 72, and 96 h) in HCT116/CDDP and HT-29/CDDP cells transfected with control, SHP2^{WT}, SHP2^{D61Y}, and SHP2^{E76K}.

Figure 3. *Continued*

(F) Colony formation capability was determined by colony formation assay in HCT116/CDDP and HT-29/CDDP cells transfected with control, $SHP2^{WT}$, $SHP2^{D61Y}$, and $SHP2^{E76K}$.

(G) Flow cytometry assays were performed to assess the apoptosis rate in HCT116/CDDP and HT-29/CDDP cells transfected with control, $SHP2^{WT}$, $SHP2^{D61Y}$, and $SHP2^{E76K}$.

(H) Expression levels of apoptotic proteins were examined and detected by western blotting in HCT116/HT-29, HCT116/CDDP, and HT-29/CDDP cells transfected with control, $SHP2^{WT}$, $SHP2^{D61Y}$, and $SHP2^{E76K}$. *$p < 0.05$, **$p < 0.01$, and ***$p < 0.001$.

$SHP2^{D61Y}$ and $SHP2^{E76K}$ inhibit CRC cell apoptosis and increase cisplatin resistance

To determine if mutations in SHP2 can influence drug resistance, we assessed their characteristics in CRC cells (HCT116 and HT-29) and CRC CDDP-resistant cells (HCT116/CDDP and HT-29/CDDP). Cell viability and OD values were significantly higher in CDDP-resistant CRC cells than in non-resistant CRC cells (Figures 3A and 3B). In HCT116/CDDP and HT-29/CDDP cells transfected with wild type (WT) or mutated SHP2, cell viability and CDDP IC_{50} values were significantly higher in cells expressing $SHP2^{D61Y}$ and $SHP2^{E76K}$ than in those expressing $SHP2^{WT}$ or the control (Figures 3C and 3D). The CDDP resistance found in cells expressing $SHP2^{E76K}$ was higher than in cells expressing $SHP2^{D61Y}$. This indicates that both mutations contribute to CDDP resistance, but the resistance is stronger in cells harboring the $SHP2^{E76K}$ gene. Cell viability and colony formation assays confirmed these results (Figures 3E and 3F). Moreover, the apoptotic rate was lower in cells expressing $SHP2^{D61Y}$ and $SHP2^{E76K}$ (Figure 3G). The levels of apoptotic proteins (Bcl-2, Bax, p21, and E2F1) measured by western blotting indicated that $SHP2^{D61Y}$ and $SHP2^{E76K}$ inhibited apoptosis (Figure 3H). Bcl-2 binds to and inactivates Bax and other pro-apoptotic proteins to prevent apoptosis, therefore higher levels of Bcl-2 indicate lower levels of apoptosis. Levels of Bcl-2 and E2F1 are higher in $SHP2^{D61Y}$ and $SHP2^{E76K}$ than in the control and $SHP2^{WT}$ transfected cells whereas levels of Bax and p21 are lower.

$SHP2^{D61Y}$ and $SHP2^{E76K}$ promote cisplatin resistance and liver metastasis of CRC *in vivo*

To evaluate the *in vivo* effects of the SHP2 mutations, we first created the *in situ* tumor model in mice using HCT116 cells/HT-29 cells transfected with control or $SHP2^{WT}$, $SHP2^{D61Y}$, and $SHP2^{E76K}$ with or without CDDP treatment. The results indicated that $SHP2^{E76K}$ and $SHP2^{D61Y}$ resulted in the promotion on tumor growth; meanwhile; $SHP2^{E76K}$ and $SHP2^{D61Y}$ could alleviate the inhibition of CDDP on the tumor growth (Figures S1A and S1B). And then, a liver metastasis model in mice using HCT116 cells transfected with control or $SHP2^{WT}$, $SHP2^{D61Y}$, and $SHP2^{E76K}$ are created. Mice were microinjected orthotopically with the cells in the tail part of the spleen. They were euthanized 5 weeks after the injection and livers were excised to assess metastasis. Representative images of tumors excised from livers are shown in Figure 4A. The growth curves and tumor weights indicate that CRC cells containing $SHP2^{E76K}$ resulted in the largest tumors and those containing $SHP2^{D61Y}$ produced the second largest tumors (Figure 4B). We confirmed that apoptosis was inhibited in $SHP2^{D61Y}$ and $SHP2^{E76K}$ tumor tissue by the low apoptotic index obtained from terminal deoxynucleotidyl transferase-mediated dUTP-biotin nick end labeling assay (TUNEL) staining and a high positive rate of Ki67 stained cells (Figure 4C). The number of hepatic metastatic nodules was higher in the xenograft tumor models injected with cells transfected with $SHP2^{D61Y}$ and $SHP2^{E76K}$ and hematoxylin and eosin (H&E) staining revealed more aggressive cancerous tissue with a disorganized structure (Figure 4D). A similar pattern emerged in mice treated with CDDP (Figures 4E–4H). Mice injected with $SHP2^{WT}$ CRC cells responded well to CDDP, whereas those injected with $SHP2^{D61Y}$ and $SHP2^{E76K}$ cells showed the greatest resistance, resulting in a significantly lower apoptotic level and a higher level of metastatic nodules. Overall, these results provide evidence that $SHP2^{D61Y}$ and $SHP2^{E76K}$ increase CDDP resistance and hepatic metastasis *in vivo*.

Regulation of PKM2 nuclear translocation by SHP2 mutations in colorectal cancer: Beyond ERK dependency

A previous study revealed that ERK1/2 phosphorylates PKM2 at Ser37 and recruits importin α5 to promote PKM2 translocation into the nucleus upon EGFR activation.[18] Therefore, we determined whether SHP2 was involved in the phosphorylation and nuclear translocation of PKM2. First, we discovered that SHP2 interacted with PKM2 in immunoprecipitation assays, indicating that SHP2 could bind to PKM2 (Figure 5A). Next, SHP2 and PKM2 mRNA and protein levels were measured in HCT116 and HT-29 cells transfected with $SHP2^{WT}$, $SHP2^{D61Y}$, and $SHP2^{E76K}$ (Figure 5B). Levels of SHP2 were highest in CRC cells transfected with $SHP2^{E76K}$ and SHP2 expression was higher in cells transfected with $SHP2^{D61Y}$ than in cells transfected with $SHP2^{WT}$. Simultaneously, the levels of PKM2 were positively influenced by specific SHP2 mutations. The highest levels of PKM2 were found in cells containing the highest level of SHP2. To determine the cellular location of SHP2 and PKM2 we used lamin B1 and β-actin as nuclear and cytoplasmic markers, respectively. Western blotting and immunofluorescent images demonstrated that although the majority of the PKM2 and SHP2 proteins were located in the cytosol, the mutations $SHP2^{D61Y}$ and $SHP2^{E76K}$ allowed a greater level of both proteins to be translocated into the nucleus (Figures 5C and 5D). To characterize the involvement of ERK in the nuclear translocation of PKM2, we also measured the phosphorylation levels of PKM2, ERK1T202/Y204, and ERK2T185/Y187 (ERK1/2) in subcellular locations in both CRC cell types (Figure 5E). Analysis with immunohistochemistry confirmed the high levels of PKM2 protein expression in CRC tissues compared to normal tissues, and indicated that SHP2 mutations promotes the cytoplasmic-to-nuclear translocation of PKM2 in CRC (Figure 5F). Phosphorylated PKM2 and ERK1/2 are found at higher levels in the cytoplasm and nucleus of HCT116 and HT-29 harboring $SHP2^{D61Y}$ and $SHP2^{E76K}$ mutations. To determine whether the PKM2 translocation was dependent on ERK phosphorylation, we measured the levels of PKM2 and ERK1/2 phosphorylation in CRC cells with or without the ERK1/2-specific inhibitor, PD98059 (Figure 5G). PD98059 reduces the phosphorylation form of *p*-PKM2, total PKM2 in both the cytosol and the nucleus, and phosphorylation form of ERK expression levels but does not affect total ERK expression level. This indicates that PKM2 expression is regulated by ERK,

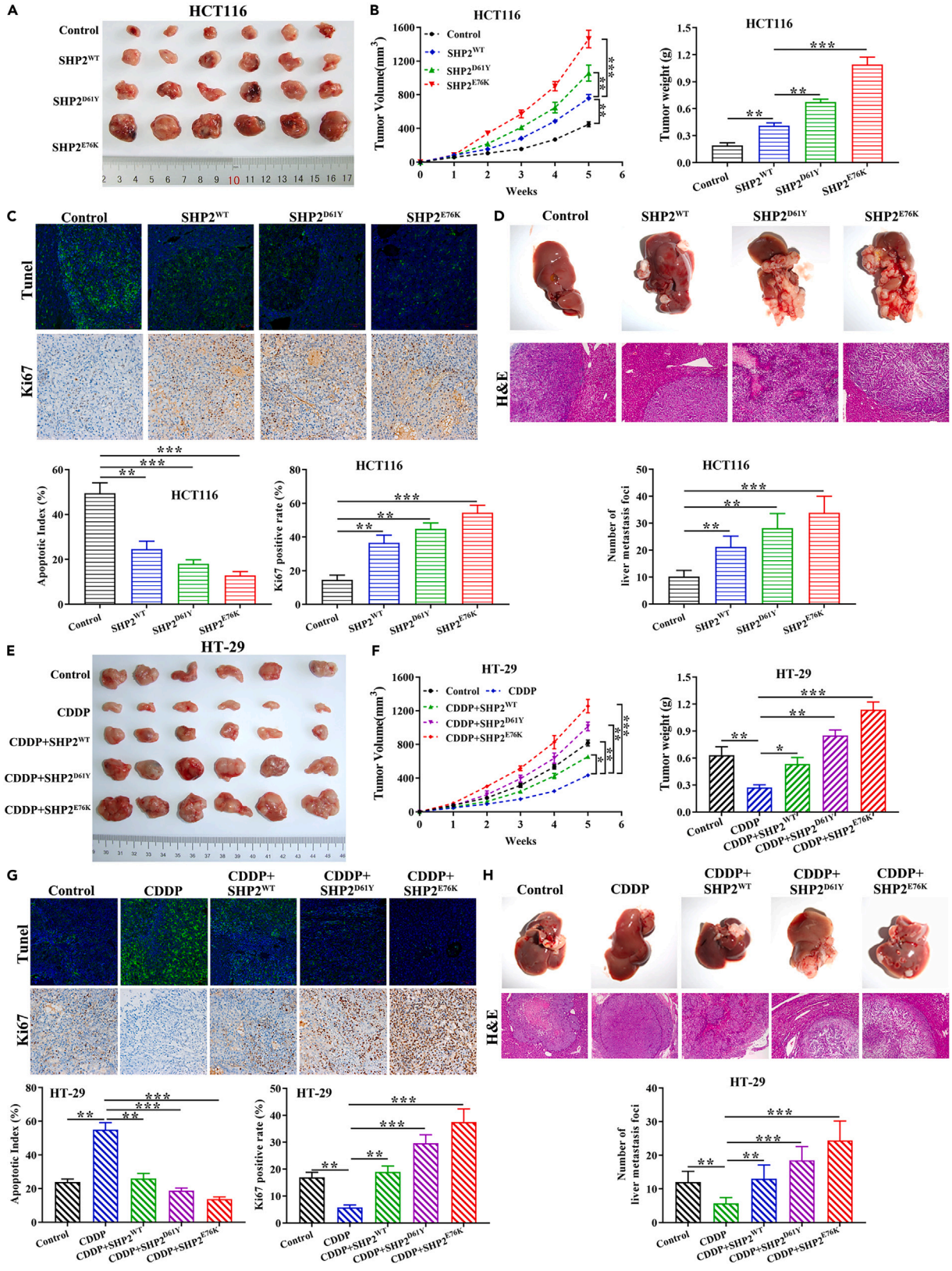
A
HCT116
Control
SHP2WT
SHP2D61Y
SHP2E76K
B
HCT116
Control
SHP2WT
SHP2D61Y
SHP2E76K
Tumor Volume(mm3)
Weeks
HCT116
Tumor weight (g)
C
Control
SHP2WT
SHP2D61Y
SHP2E76K
Tunel
Ki67
HCT116
Apoptotic Index (%)
HCT116
Ki67 positive rate (%)
HCT116
Number of liver metastasis foci
D
Control
SHP2WT
SHP2D61Y
SHP2E76K
H&E
E
HT-29
Control
CDDP
CDDP+SHP2WT
CDDP+SHP2D61Y
CDDP+SHP2E76K
F
HT-29
Control
CDDP
CDDP+SHP2WT
CDDP+SHP2D61Y
CDDP+SHP2E76K
Tumor Volume(mm3)
Weeks
HT-29
Tumor weight (g)
G
Control
CDDP
CDDP+ SHP2WT
CDDP+ SHP2D61Y
CDDP+ SHP2E76K
Tunel
Ki67
HT-29
Apoptotic Index (%)
HT-29
Ki67 positive rate (%)
H
Control
CDDP
CDDP+ SHP2WT
CDDP+ SHP2D61Y
CDDP+ SHP2E76K
H&E
HT-29
Number of liver metastasis foci

Figure 4. SHP2^{D61Y} and SHP2^{E76K} promoted cisplatin (CDDP) resistance and liver metastasis of colorectal cancer (CRC) *in vivo*

(A and B) HCT116 cells transfected with control, SHP2^{WT}, SHP2^{D61Y}, and SHP2^{E76K} were orthotopically microinjected in the tail part of the spleen of mice to generate the liver metastasis model. At 5 weeks after the intrasplenic injection, all mice were euthanized and livers were excised to assess metastasis. Representative images of tumors with tumor volumes and tumor weights were quantified and shown.

(C) TUNEL staining and Ki67 immunohistochemistry demonstrate the apoptotic Index and Ki67 positive rate in the indicated tissues from mice with HCT116 cells transfected with Control or SHP2^{WT}, SHP2^{D61Y}, and SHP2^{E76K}, and the quantified results are also shown.

(D) Number of hepatic metastatic nodules and H&E staining of hepatic metastasis nodules in the xenograft tumor models in the indicated tissues and the quantified results are also shown.

(E and F) HT-29 cells were transfected with control or SHP2^{WT}, SHP2^{D61Y}, and SHP2^{E76K} after treatment with CDDP, and then the cells were orthotopically microinjected in the tail part of the spleen to generate the liver metastasis model. At 5 weeks after the intrasplenic injection, all mice were euthanized and livers were excised by dissection to assess metastasis. Representative images of tumors with tumor volumes and tumor weights were quantified and shown.

(G) TUNEL staining and Ki67 immunohistochemistry demonstrate the expression of apoptotic Index and Ki67 positive rate in the indicated tissues from mice with HT-29 cells transfected with Control or SHP2^{WT}, SHP2^{D61Y}, SHP2^{E76K} after treatment with cisplatin. Quantitative analysis of the levels from liver metastasis tumor sections in different cells per field was calculated with ImageJ software.

(H) Number of liver tumor metastatic foci and H&E staining of hepatic metastasis nodules in the xenograft tumor models, and the quantified results are also shown. *$p < 0.05$, **$p < 0.01$, and ***$p < 0.001$.

whereas PKM2 nuclear localization depends on SHP2 mutation. Glucose consumption, lactate production, and ATP levels in HCT116 cells that were increased by SHP2 mutations were reduced to control levels when PD98059 is applied (Figure 5H), indicating that the inhibition of ERK phosphorylation prevents glycolysis in CRC cells. CRC cells containing SHP2 mutations were also treated with a PKM2-specific inhibitor (PKM2-IN-1). PKM2-IN-1 reduces the phosphorylation form of PKM2 and total PKM2 expression levels but does not affect *p*-ERK and ERK expression levels (Figure 5I). Glucose consumption, lactate production, and ATP levels in HT-29 cells transfected with SHP2^{D61Y} and SHP2^{E76K} were elevated but when PKM2 is inhibited, levels return to those of the control (Figure 5J). This indicates that along with ERK phosphorylation, PKM2 influences glycolysis in CRC cells. While ERK activity influences PKM2 expression, our data suggest that the nuclear translocation of PKM2, promoted by SHP2^{D61Y} and SHP2^{E76K}, does not depend solely on ERK phosphorylation, indicating the involvement of other regulatory mechanisms.

SHP2^{D61Y} and SHP2^{E76K} promote CRC cell proliferation and glycolysis through PKM2 nuclear translocation

The mRNA expression of PKM2 was determined in the tumor tissue of patients with CRC ($n = 35$), CRC liver metastasis ($n = 12$), and normal tumor-adjacent tissues ($n = 47$) (Figure 6A). The expression of PKM2 was significantly higher in CRC tissue than in normal tissue with the highest expression observed in CRC tissue with metastasis. The expression of PKM2 was also higher in CRC cells (HT29, W480, VAC0432, and HCT116) compared to normal cells (HCoEpiC) (Figure 6B), and the highest expression was found in HCT116 cells. PKM2 was overexpressed and silenced in HCT116 and HT-29 cells harboring the SHP2^{D61Y} and SHP2^{E76K} mutations (Figures 6C and 6D). The lowest levels of proliferation and colony formation were found in CRC cells with PKM2 silenced; however, SHP2^{D61Y} and SHP2^{E76K} increased the levels of CRC cell proliferation. Relative glucose uptake and lactate production were decreased in PKM2 knockdown HCT116 cells and increased in PKM2 overexpressing HT-29 cells; however, these effects were alleviated by the addition of SHP2^{D61Y} and SHP2^{E76K} in PKM2 knockdown HCT116 cells, and aggravated by the addition of SHP2^{D61Y} and SHP2^{E76K} in PKM2 overexpressing HT-29 cells (Figure 6E). Glycolysis was further characterized using extracellular acidification rate (ECAR) and levels of glycolytic enzymes (Figures 6F–6H). It was confirmed that the silencing of PKM2 could prevent proliferation and glycolytic characteristics in CRC cells.

PKM2 increases CRC cell proliferation and migration/invasion by regulating hnRNPK ubiquitination

Related studies reported that hnRNPK is an important RNA and DNA binding protein that regulates a variety of biological activities, including CRC[21]; PKM2 expression and its nuclear translocation depend on the activation of the mitogen-activated protein kinase (MEK)/extracellular signal-regulated kinase (ERK) pathway,[8] and that the MEK/ERK signaling pathway favors the phosphorylation of hnRNPK and promotes hnRNPK activation.[22] Moreover, starbase 3.0 predicted that PKM2 could bind to hnRNPK and regulates its expression. (https://rnasysu.com/encori/). Therefore, we examined the expression of hnRNPK in relation to the SHP2 mutations and PKM2. Co-immunoprecipitation revealed that PKM2 and hnRNPK interact in CRC cells (Figure 7A) and this was confirmed by immunofluorescence images (Figure 7B). We then determined the expression of hnRNPK in cells overexpressing or inhibiting the expression of PKM2 (Figure 7C). The suppression of PKM2 expression also inhibited the expression of hnRNPK. The degradation of the hnRNPK protein in PKM2 knockdown CRC cells was measured by CHX chase analysis (Figures 7D and 7E). The levels of hnRNPK are lower in cells with PKM2 expression inhibited, signifying that PKM2 regulates the ubiquitination of hnRNPK. To analyze the ubiquitination of hnRNPK further, HCT116 cells were treated with MG132 (5 μM) for 8 h (Figure 7F). The protein expression of PKM2 and hnRNPK examined by western blotting revealed that PKM2 knockdown reduced the levels of hnRNPK, which were alleviated by adding the specific proteasome inhibitor MG132 to HCT116 cells. The ubiquitination of hnRNPK was also examined when PKM2 was knocked down in HCT116 and HT-29 cells. The ubiquitination of hnRNPK was tested by immunoprecipitation and analyzed by anti-ubiquitin antibody using western blotting (Figure 7G). The results confirmed that the ubiquitination level of hnRNPK was significantly decreased by PKM2 knockdown in the presence of MG132. These results confirm that PKM2 is responsible for ubiquitinating hnRNPK. In CRC cells co-transfected with shNC/shPKM2 and hnRNPK or with mock/PKM2 and sh-hnRNPK, the inhibition of PKM2 resulted in higher levels of apoptosis in CDDP-treated cells (Figure 7H). Apoptosis was higher and the migration and invasion of CRC cells were lower

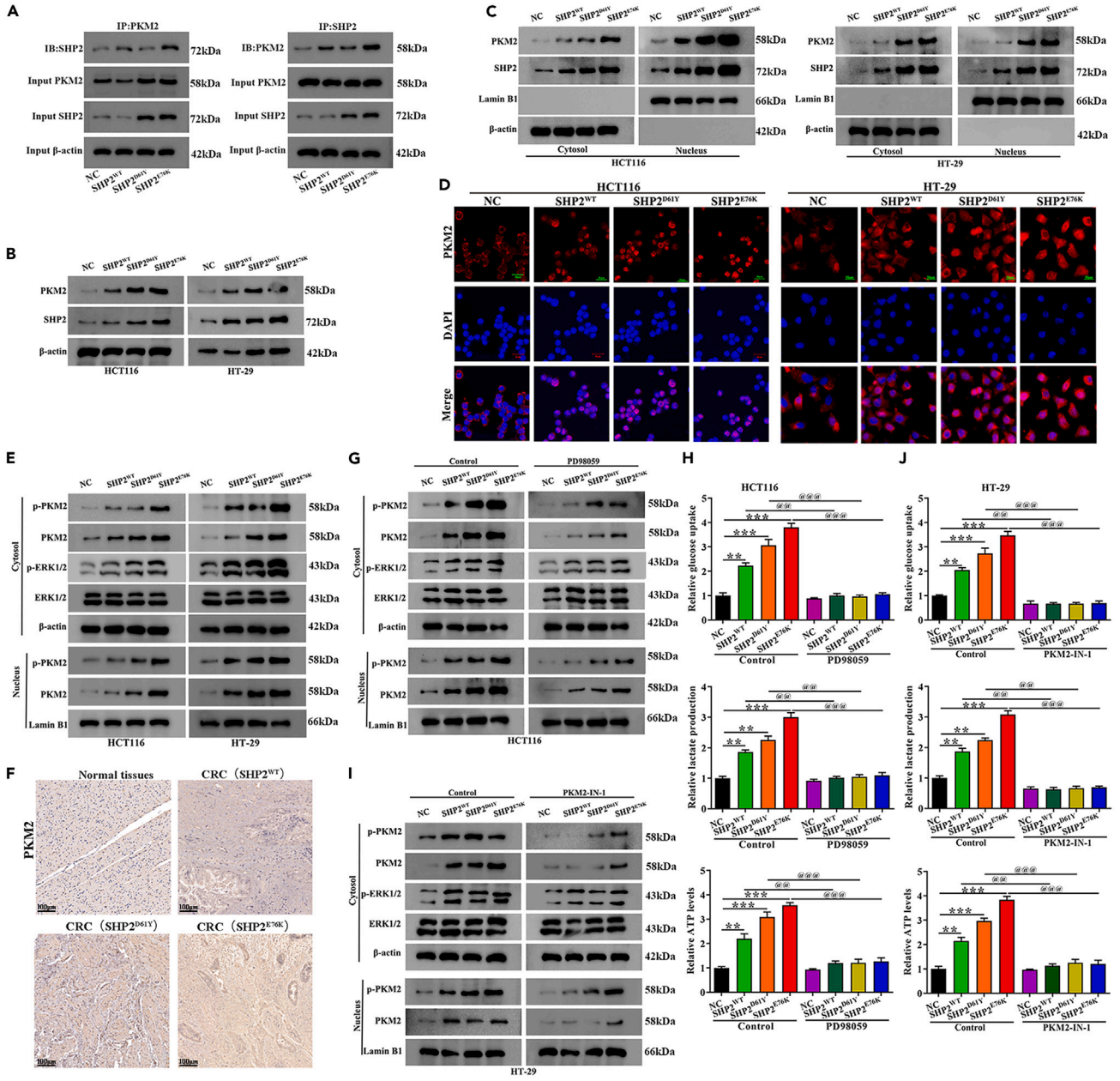

Figure 5. Regulation of PKM2 nuclear translocation by SHP2 mutations in colorectal cancer: beyond ERK dependency

(A) Proteins from stable HT29 cells or control cells were immunoprecipitated using an anti-PKM2 antibody (left) and anti-SHP2 antibody (right); immunoblotting performed with an anti-SHP2 antibody (left) and anti-PKM2 antibody (right) were shown.

(B) SHP2 and PKM2 mRNA and protein levels were detected by qRT-PCR and western blotting in HCT116 and HT-29 cells, transfected with control and $SHP2^{WT}$, $SHP2^{D61Y}$, and $SHP2^{E76K}$.

(C) Nuclear and cytosolic protein lysates prepared from HCT116 and HT-29 cells stably expressing control or $SHP2^{WT}$, $SHP2^{D61Y}$, and $SHP2^{E76K}$ were assayed by western blotting, lamin B1 were as the nucleus control and β-actin were as cytosol control.

(D) The subcellular localization of PKM2 in HCT116 and HT-29 cells stably expressing control or $SHP2^{WT}$, $SHP2^{D61Y}$, and $SHP2^{E76K}$ was visualized by immunofluorescence assay.

(E) Phosphorylation of $PKM2^{S37}$, total PKM2 and phosphorylation of $ERK1^{T202/Y204}$/$ERK2^{T185/Y187}$ and total $ERK1^{T202/Y204}$/$ERK2^{T185/Y187}$ in CRC cells stably expressing control or $SHP2^{WT}$, $SHP2^{D61Y}$, $SHP2^{E76K}$, cytosolic and nuclear lysates were prepared, subsequently detected by western blotting.

(F) PKM2 protein expression in normal tissues and CRC tissues ($SHP2^{WT}$, $SHP2^{D61Y}$ and $SHP2^{E76K}$) was determined by immunohistochemistry.

(G and H) HCT116 cells were transfected with control (NC), $SHP2^{WT}$, $SHP2^{D61Y}$, and $SHP2^{E76K}$ and/or treated with the ERK inhibitor PD98059 (10 μM) for 24 h. And phosphorylation of $PKM2^{S37}$, total PKM2, phosphorylation of $ERK1^{T202/Y204}$/$ERK2^{T185/Y187}$, total $ERK1^{T202/Y204}$/$ERK2^{T185/Y187}$ were detected by western blotting

Figure 5. *Continued*

analysis, lamin B1 were as the nucleus control and β-actin were as cytosol control. glucose uptake, lactate production, and ATP levels were also examined and shown.

(I and J) HT-29 cells were transfected with control (NC), $SHP2^{WT}$, $SHP2^{D61Y}$, and $SHP2^{E76K}$ and/or treated with the PKM2 inhibitor PKM2-IN-1 (9 μM) for 24 h. And phosphorylation of $PKM2^{S37}$, total PKM2, phosphorylation of $ERK1^{T202/Y204}$/$ERK2^{T185/Y187}$, total $ERK1^{T202/Y204}$/$ERK2^{T185/Y187}$ were detected by western blotting analysis, lamin B1 were as the nucleus control and β-actin were as cytosol control. glucose uptake, lactate production, and ATP levels in HT-29 cells are shown. *$p < 0.05$, **$p < 0.01$, and ***$p < 0.001$.

in response to CDDP when PKM2 was silenced. However, the overexpression of hnRNPK under these conditions led to lower levels of apoptosis and increases in migration and invasion (Figures 7I and 7J). Moreover, we detected the effect of hnRNPK knockdown and overexpression on cell proliferation in HCT116 and HT-29 cells. The results indicated that hnRNPK knockdown could inhibit CRC cell proliferation and migration/invasion; whereas, hnRNPK overexpression has an opposite result in CRC cells (Figures S2A and S2B). These results confirm that PKM2 increases CRC cell proliferation and migration/invasion by regulating hnRNPK ubiquitination.

$SHP2^{D61Y}$ and $SHP2^{E76K}$-mediated increases in proliferation and glycolysis are reversed by the downregulation of hnRNPK

The levels of hnRNPK mRNA and protein expression were lower in normal tumor-adjacent tissues ($n = 47$) than in tissues from patients with CRC ($n = 35$) or CRC liver metastasis ($n = 12$) (Figures 8A and 8B). The mRNA and protein levels of hnRNPK were also higher in CRC cells than in normal cells (Figure 8C). The interference and overexpression efficiency of hnRNPK was assessed and confirmed by RT-qPCR and western blotting in HCT116 cells transfected with shCtrl/sh-hnRNPK and HT-29 cells transfected with vector/hnRNPK (Figure 8D). The mRNA and protein expression levels of hnRNPK was higher in HCT116 and HT-29 cells transfected with $SHP2^{D61Y}$ than in cells transfected with $SHP2^{WT}$, and the highest expression was found in cells transfected with $SHP2^{E76K}$ (Figure 8E). In HCT116 cells co-transfected with shNC/shPKM2 and $SHP2^{WT}$/$SHP2^{D61Y}$/$SHP2^{E76K}$, the loss of PKM2 results in lower levels of hnRNPK. However, when HT-29 was co-transfected with vector/PKM2 and $SHP2^{WT}$/$SHP2^{D61Y}$/$SHP2^{E76K}$ the levels of hnRNPK increased, indicating an interaction between PKM2, SHP2, and hnRNPK (Figure 8F). The proliferation of CRC cells co-transfected with $SHP2^{WT}$/$SHP2^{D61Y}$/$SHP2^{E76K}$ and either shCtrl/sh-hnRNPK or vector/hnRNPK were compared. In cells with hnRNPK suppressed, cell proliferation was the highest when $SHP2^{E76K}$ was co-expressed with shCtrl. Interference of hnRNPK resulted in the lower proliferation of cells transfected with $SHP2^{E76K}$ (Figure 8G). The lowest proliferation occurred when $SHP2^{WT}$ and sh-hnRNPK were co-expressed. The highest proliferation occurs when hnRNPK is overexpressed in cells transfected with $SHP2^{E76K}$. Glucose uptake and lactate production were significantly lower in HCT116 and HT-29 cells transfected with $SHP2^{D61Y}$/$SHP2^{E76K}$ when hnRNPK is suppressed and higher when hnRNPK is overexpressed (Figures 8H and 8I). Levels of glycolysis, glycolytic capacity, and the expression of key glycolytic enzymes in CRC cells transfected with SHP2 mutations were also lower when hnRNPK was suppressed and higher when hnRNPK was overexpressed (Figures 8J–8L). These results demonstrate that the increases in proliferation and glycolysis mediated by $SHP2^{D61Y}$ and $SHP2^{E76K}$ are reversed by the downregulation of hnRNPK.

DISCUSSION

Mutations that promote glycolysis are frequently implicated in metastasis and drug resistance in CRC.[23–26] In this study, we have analyzed the effect of change-of-function mutations in SHP2 on glycolysis, metastasis, and drug resistance in CRC. At present, there is limited information on the relevance of SHP2 mutations in cisplatin-induced apoptosis. SHP2 is known to mediate cisplatin resistance by inhibiting apoptosis through activating the Ras/PI3K/AKT/survivin pathway in lung cancer cells.[27] We discovered that the SHP2 mutations E76K and D61Y occurred the most frequently in CRC. Patients with tumors containing either of these mutations have a worse OS than patients with wild-type SHP2. Therefore, we characterized the interactions of SHP2 containing these nonsynonymous mutations with other proteins known to promote glycolysis and cancer progression in CRC cells and a mouse model of metastasis.

While our study demonstrates that $SHP2^{D61Y}$ and $SHP2^{E76K}$ mutations promote PKM2 nuclear translocation, the precise mechanism by which SHP2 regulates this process requires further elucidation. Recent studies have revealed that PKM2 nuclear translocation can be regulated by various mechanisms. For example, DDX39B has been shown to recruit importin α5 to accelerate the nuclear translocation of PKM2 independent of ERK1/2-mediated phosphorylation of PKM2, leading to the transactivation of oncogenes and glycolysis-related genes in CRC.[10] Given that SHP2 is a multifunctional tyrosine phosphatase that can regulate various signaling pathways, we hypothesized that $SHP2^{D61Y}$ and $SHP2^{E76K}$ mutations might enhance PKM2 nuclear translocation by modulating ERK signaling, a well-known downstream pathway of SHP2. To test this hypothesis, we treated the mutant cells with an ERK inhibitor. Interestingly, while ERK inhibition reduced PKM2 expression, it did not significantly affect PKM2 nuclear localization. This suggests that SHP2 mutations may influence PKM2 nuclear translocation through mechanisms independent of the ERK signaling pathway, such as by affecting the exposure of PKM2's nuclear localization signal or its binding to nuclear transport proteins. Further studies are needed to elucidate the specific mechanisms underlying SHP2-mediated regulation of PKM2 nuclear translocation in CRC. Moreover, PKM2 nuclear translocation is typically regulated by its nuclear localization signal sequences (NLS) and interactions with nuclear transport proteins such as importin α5.[10] Whether SHP2 mutations influence PKM2 nuclear translocation by affecting the exposure of its NLS or its binding to nuclear transport proteins is an area worthy of further investigation. Future studies should focus on elucidating the specific mechanisms by which SHP2 regulates PKM2 nuclear translocation, such as identifying potential PKM2 sites phosphorylated by SHP2 and analyzing the dynamic changes in the binding partners of SHP2 and PKM2

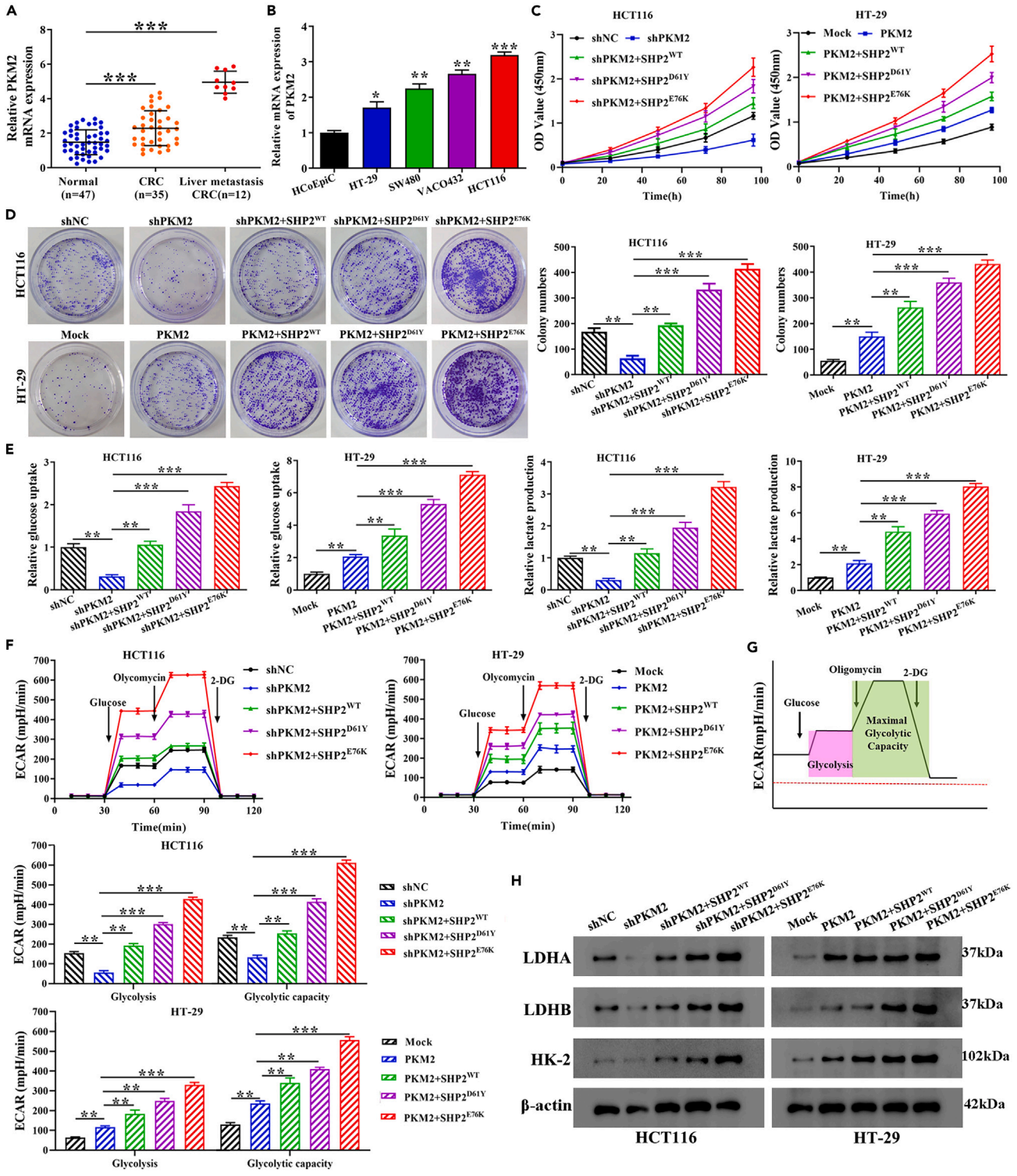

Figure 6. SHP2^{D61Y} and SHP2^{E76K} promote CRC cell proliferation and glycolysis through PKM2 nuclear translocation

(A) PKM2 mRNA expression in normal tumor-adjacent tissues, CRC, and CRC liver metastasis were detected by RT-qPCR.

(B) The mRNA levels of PKM2 in CRC cells and normal cells (HCoEpiC) were examined by RT-qPCR.

(C) The cell proliferation capability in HCT116 cells transfected or co-transfected with shNC, shPKM2, shPKM2+SHP2^{WT}, shPKM2+SHP2^{D61Y}, and shPKM2+SHP2^{E76K} were determined by CCK-8 assay; the cell proliferation capacity in HT-29 cells, which were transfected or co-transfected with Mock, PKM2, PKM2+SHP2^{WT}, PKM2+SHP2^{D61Y}, and PKM2+SHP2^{E76K} were also determined by CCK-8 assay.

Figure 6. *Continued*

(D) The colony formation capability in HCT116 cells, which were transfected or co-transfected with shNC, shPKM2, shPKM2+SHP2^{WT}, shPKM2+SHP2^{D61Y}, and shPKM2+SHP2^{E76K} were determined by colony formation assays; the colony formation capability in HT-29 cells, which were transfected or co-transfected with Mock, PKM2, PKM2+SHP2^{WT}, PKM2+SHP2^{D61Y}, and PKM2+SHP2^{E76K} were determined by colony formation assays. The quantitative results were also shown

(E) glucose uptake and lactate production were examined in HCT116 cells transfected or co-transfected with shNC, shPKM2, shPKM2+SHP2^{WT}, shPKM2+SHP2^{D61Y}, shPKM2+SHP2^{E76K} and HT-29 cells transfected or co-transfected with mock, PKM2, PKM2+SHP2^{WT}, PKM2+SHP2^{D61Y}, PKM2+SHP2^{E76K}.

(F) Extracellular acidification rate (ECAR) was determined by Seahorse XF assays in HCT116 cells transfected or co-transfected with shNC, shPKM2, shPKM2+SHP2^{WT}, shPKM2+SHP2^{D61Y}, shPKM2+SHP2^{E76K} and HT-29 cells transfected or co-transfected with Mock, PKM2, PKM2+SHP2^{WT}, PKM2+SHP2^{D61Y}, PKM2+SHP2^{E76K}.

(G) ECAR experimental protocol, glycolysis (pink), and maximal glycolytic capacity (green) were quantified and shown of Figure 6F.

(H) The expression levels of key glycolytic enzymes were determined by western blotting in HCT116 cells transfected or co-transfected with shNC, shPKM2, shPKM2+SHP2^{WT}, shPKM2+SHP2^{D61Y}, shPKM2+SHP2^{E76K}, and HT-29 cells transfected or co-transfected with mock, PKM2, PKM2+SHP2^{WT}, PKM2+SHP2^{D61Y}, PKM2+SHP2^{E76K}. *$p < 0.05$, **$p < 0.01$, and ***$p < 0.001$.

in the presence of SHP2 mutations. These studies will contribute to a better understanding of the role of SHP2 in CRC progression and may lead to the discovery of novel therapeutic targets.

In this study, we found that both E76K and D61Y mutations in SHP2 caused an increased level of proliferation and migration and reduced apoptosis in CRC cells but the E76K mutation had the greatest impact. In addition, SHP2^{E76K} and SHP2^{D61Y} appeared to induce glycolysis and promote drug resistance, with SHP2^{E76K} generating the highest levels. The gain-of-function mutation SHP2^{E76K} resulted in more aggressive characteristics in CRC cells. In a mouse model of liver metastasis, SHP2^{E76K} gave rise to higher levels of metastatic nodules than SHP2^{D61Y} *in vivo* and contributed to the greatest level of CDDP resistance. Gain-of-function mutations in SHP2 are known to aggravate several health conditions including cancer by enhancing the activities of ERK and AKT kinases and the Wnt/β-catenin signaling pathway.[17,28] Similar results to ours were obtained in a recent study,[17] the SHP2^{E76K} mutation was found to act as an oncogene in colitis-associated CRC by inducing the Wnt/β-catenin signaling pathway and promoting tumorigenesis and metastasis. In a molecular dynamics study, Li et al. propose that the E76K mutation increases the activity of SHP2 because of a large variation in two regions of amino acids (Y81–Q83 and Q258–L261), which affects the stability of the protein.[29] A structural study by LaRochelle et al. discovered that SHP2^{E76K} adopted an open structure whereas the structure of SHP2^{WT} was closed.[30] The open structure of SHP2^{E76K} exposes the active site; however, when bound to the allosteric inhibitor SHP099, SHP2^{E76K} reverts to a similar conformation as SHP2^{WT}.

SHP2 regulates several pathways that are involved in drug resistance, such as ERK, JAK-STAT, and PI3K-AKT,[31–33] and is recognized as a potential target in the management of cancer.[34–36] Zheng et al. found that, SHP2^{E76K} activation enhances ERK and AKT activities in forebrain progenitor cells, and levels of SHP2 activating mutations correlated with the potency of the enhanced SHP2 catalytic activity.[28] Nabinger et al. found that the apparent functional difference between SHP2^{D61Y}, which induces myeloproliferative disorders (MPD) but fails to induce acute leukemia, and SHP2^{E76K}, which can induce leukemia of various lineages, may be due to the increased phosphatase activity of SHP2^{E76K}. SHP2^{E76K} is known to have the highest phosphatase activity of the various gain-of function Shp2 mutants tested.[37] Due to the difference in the phosphatase activity associated with SHP2^{D61Y} and SHP2^{E76K}, we hypothesized that SHP2^{D61Y} may have different effects on the ERK and AKT activities compared to SHP2^{E76K}. This deserves to be explored in depth by future studies.

After establishing that nonsynonymous mutations in SHP2 could promote glycolysis, metastasis, and drug resistance in CRC cells, we examined the interactions and pathways of SHP2 in more detail. In a previous study, ERK1/2 was found to phosphorylate PKM2 at Ser37 to promote its translocation into the nucleus upon EGFR activation.[18] In the nucleus, PKM2 is believed to promote the transcription of oncogenes and glycolysis-related genes to generate the Warburg effect in CRC.[10] In this study, the inhibition of PKM2 prevents the glycolysis promoted by SHP2^{D61Y} and SHP2^{E76K} and reduces glucose uptake and lactate production in CRC cells. We found that SHP2^{D61Y} and SHP2^{E76K} promote glycolysis by accelerating the nuclear translocation of PKM2 in an ERK1/2-dependent manner. Therefore, increased interactions between ERK1/2 and PKM2 caused by the phosphatase activity of SHP2 results in the increased translocation of PKM2. In prostate cancer, it has been found that cullin 3/SPOP, an E3 ubiquitin ligase complex, promotes the degradation of hnRNPK and, in turn, ERK1/2 can inhibit cullin 3/SPOP.[38,39] This initially indicates that the exact interactions between SHP2, ERK1/2, and hnRNPK. Moreover, the mechanism of SHP2 mutation and ERK in the translocation of PKM2 is multifaceted and not very clear, and the underlying mechanism requires clarification in further studies, and this also is a limitation of our manuscript, which need the in-depth studies. Taken together, our results confirm those found in previous studies, gain-of-function mutations that promote PKM2 translocation into the nucleus can enhance glycolysis and tumor metastasis.[18,40,41]

The post-translational modification of hnRNPK through processes such as ubiquitination is known to promote several cellular functions, such as proliferation and apoptosis, and is implicated in tumorigenesis.[42] We found that PKM2 upregulates the expression of hnRNPK and decreases its degradation. Lower levels of hnRNPK ubiquitination increase cell proliferation. The regulation of hnRNPK ubiquitination is known to promote several other cancers, including prostate tumorigenesis and breast cancer metastasis.[12,39] In prostate cancer, the overexpression of hnRNPK caused by a lack of degradation promotes the progression of tumorigenesis.[39] In breast cancer, an interaction between PROX1 and hnRNPK was found to prevent hnRNPK ubiquitination,[12] which, in turn, activated Wnt/β-catenin signaling and promoted metastasis. Therefore, SHP2^{D61Y} and SHP2^{E76K} enhance glycolysis, cell proliferation, and migration, and lower CDDP-induced apoptosis through PKM2/hnRNPK signaling. We found that the downregulation of hnRNPK reverses the promotion of glycolysis and increases cancer cell sensitivity to CDDP. However, the more detailed mechanism of PKM2 regulates hnRNPK stability through ubiquitination modification remains to be studied in depth, and it also provides direction and ideas for the next research.

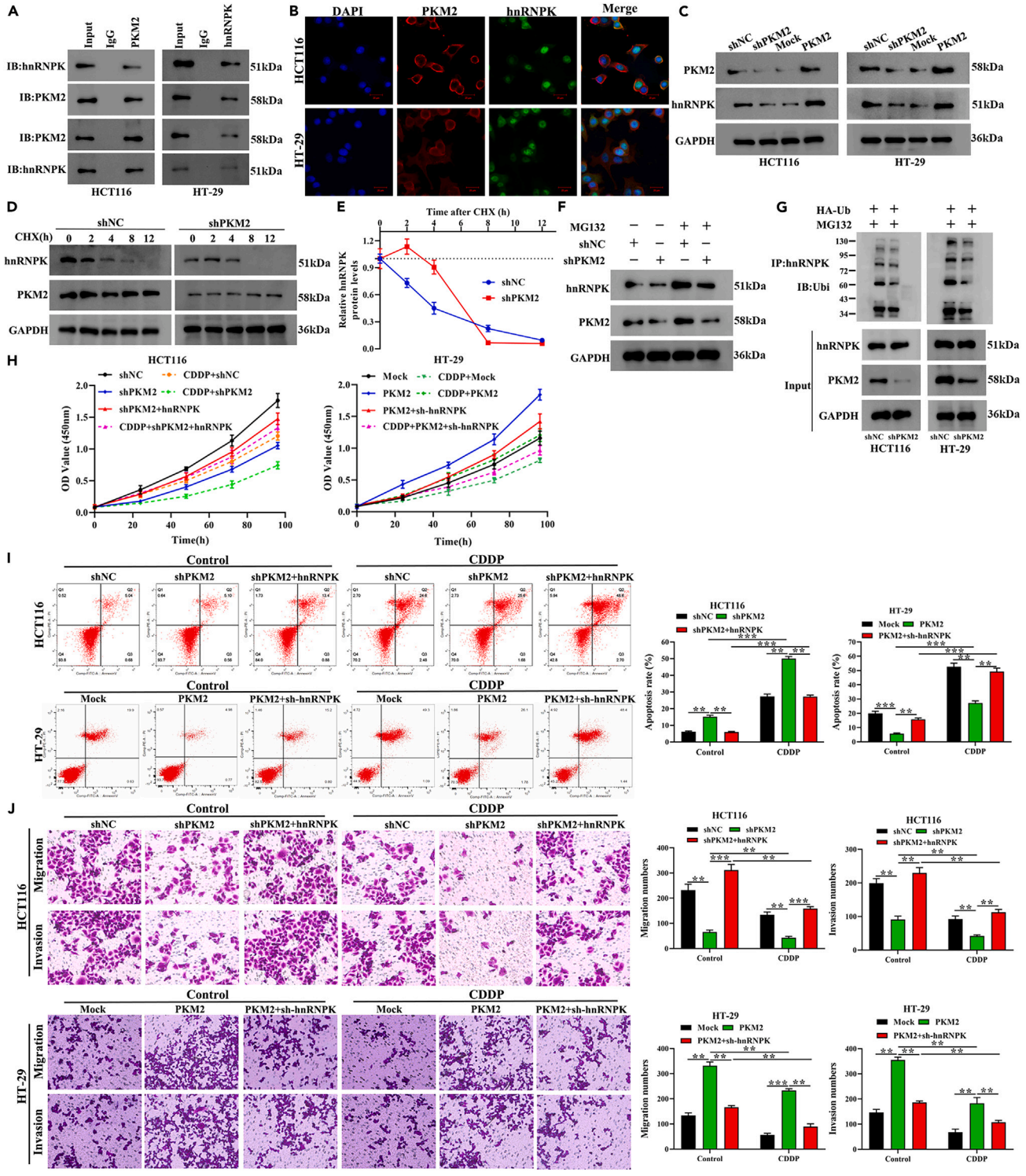

Figure 7. PKM2 interacts with hnRNPK and increases CDDP-mediated CRC cell proliferation and migration/invasion by regulating hnRNPK ubiquitination

(A) Co-immunoprecipitation analysis of the interaction between PKM2 and hnRNPK in HCT116 and HT-29 cells and the results were shown.

(B) Co-localization of PKM2 (green) and hnRNPK (red) were indicated by immunofluorescence confocal microcopy. DAPI was used for nuclear staining (blue).

(C) Expression levels of hnRNPK in PKM2-knockdown and overexpressing HCT116/HT-29 cells were determined by western blotting.

Figure 7. *Continued*

(D and E) HCT116 cells transfected with shNC or shPKM2 were treated with Cycloheximide (CHX, 100 μg/ml), and cells were harvested at the indicated time points (0, 2, 4, 8, and 12 h). The protein expression levels of PKM2 and hnRNPK were examined by western blotting. Quantification of hnRNPK protein levels were determined using ImageJ software normalized to GAPDH and shown.

(F) MG132 (5 μM) contact with HCT116 cells transfected with shNC or shPKM2 for 8 h, and then the protein expression of PKM2 and hnRNPK were examined by western blotting, and GAPDH as the control.

(G) The ubiquitination of hnRNPK was examined with PKM2 knocked down in HCT116 and HT-29 cells. Ubiquitin-HA was transfected into shNC and shPKM2 HCT116/HT-29 cells. Ubiquitination hnRNPK was tested by IP of hnRNPK and analyzed by anti-ubiquitin antibody with western blotting.

(H–J) HCT116 cells were transfected or co-transfected with shNC, shPKM2, and shPKM2+hnRNPK; while HT-29 were transfected or co-transfected with Mock, PKM2 and PKM2+sh-hnRNPK, after CDDP treatment or un-treatment (48 h). Cell proliferation was determined by CCK-8 assays. Cell apoptosis was detected by flow cytometry assays, and the quantitative results were also sown.

(J) HCT116 cells were transfected or co-transfected with shNC, shPKM2, and shPKM2+hnRNPK; while HT-29 cells were transfected or co-transfected with mock, PKM2 and PKM2+sh-hnRNPK, after CDDP treatment or un-treatment (48 h). Cell migration/invasion were detected by transwell assays, and the quantitative results were also sown. $*p < 0.05$, $**p < 0.01$, and $***p < 0.001$.

In conclusion, our study demonstrates that mutations in SHP2, particularly $SHP2^{E76K}$ and $SHP2^{D61Y}$, result in increased phosphatase activity and promote a more aggressive form of CRC in a mouse model of liver metastasis compared to $SHP2^{WT}$. Mechanistically, we found that these SHP2 mutations promote glycolysis by accelerating the nuclear translocation of PKM2, a key glycolytic enzyme. Interestingly, while we initially hypothesized that SHP2 mutations might enhance PKM2 nuclear translocation by increasing ERK1/2 activity, our data suggest that SHP2 may regulate this process through alternative mechanisms, such as by affecting the exposure of PKM2's nuclear localization signal or its binding to nuclear transport proteins. Once in the nucleus, PKM2 enhanced the levels of hnRNPK, a key transcriptional coactivator, and increased CRC cell proliferation and migration/invasion via the regulation of hnRNPK ubiquitination. Our findings provide new insights into the molecular mechanisms underlying CRC progression and highlight the crucial role of SHP2 mutations in promoting PKM2 nuclear translocation. However, further research is needed to fully elucidate the specific mechanisms by which SHP2 regulates PKM2 nuclear translocation. Future studies should focus on identifying the PKM2 sites phosphorylated by SHP2, analyzing the dynamic changes in the binding partners of SHP2 and PKM2 in the presence of SHP2 mutations, and exploring other potential mechanisms, such as the regulation of PKM2 post-translational modifications, protein-protein interactions, nucleocytoplasmic transport pathways, and epigenetic modifications. These studies will not only deepen our understanding of the role of SHP2 and PKM2 in CRC but also contribute to the discovery of novel therapeutic targets and provide new strategies for the precision treatment of CRC.

Conclusion

In conclusion, our study demonstrates that SHP2 mutations, particularly $SHP2^{D61Y}$ and $SHP2^{E76K}$, promote a more aggressive form of CRC by enhancing glucose metabolism, cell proliferation, migration, and invasion, as well as preventing CDDP-induced apoptosis. Mechanistically, these SHP2 mutations facilitate the nuclear translocation of PKM2, a key glycolytic enzyme, which subsequently activates the PKM2/hnRNPK signaling pathway. These findings provide new insights into the molecular mechanisms underlying the aggressive progression of CRC with SHP2 mutations and highlight the crucial role of PKM2 nuclear translocation in this process. Targeting PKM2 nuclear translocation or its interaction with hnRNPK may represent a promising strategy to attenuate the aggressive phenotypes driven by SHP2 mutations in CRC. Our findings contribute to a better understanding of the complex role of SHP2 and PKM2 in CRC and may have important implications for the development of personalized therapies for CRC patients harboring SHP2 mutations.

STAR★METHODS

Detailed methods are provided in the online version of this paper and include the following:

- KEY RESOURCES TABLE
- RESOURCE AVAILABILITY
  - Lead contact
  - Materials availability
  - Data and code availability
- EXPERIMENTAL MODEL AND STUDY PARTICIPANT DETAILS
  - Ethics approval and consent to participate
  - Human materials
  - Animals
- METHOD DETAILS
  - Clinical samples
  - Cell culture and transfection
  - Quantitative RT-PCR
  - Western blot analysis
  - Cell counting assay

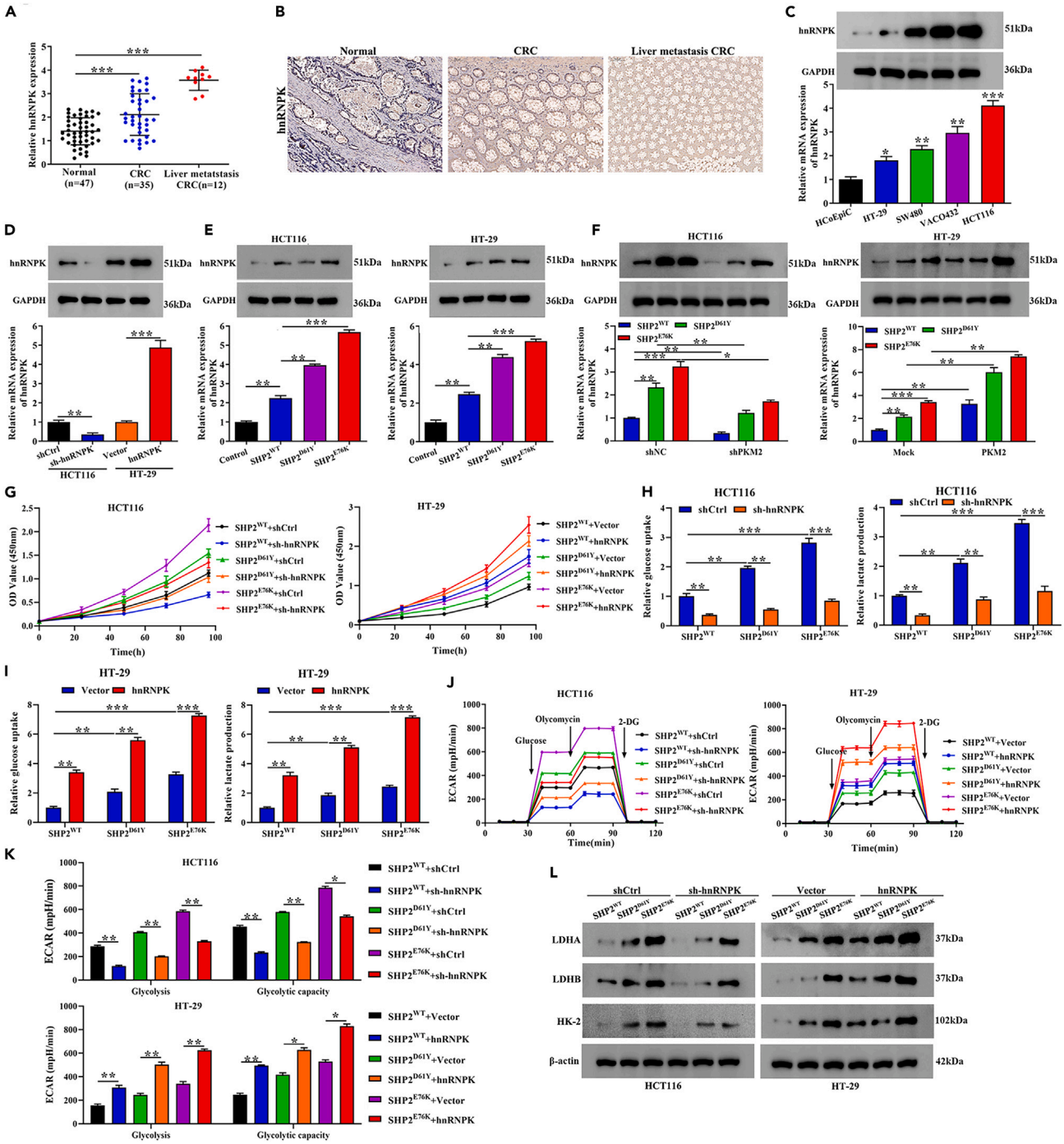

Figure 8. SHP2^{D61Y} and SHP2^{E76K} effects on proliferation and glycolysis are reversed by the downregulation of hnRNPK

(A) hnRNPK mRNA expression in normal tumor-adjacent tissues, CRC, and CRC liver metastasis was detected by RT-qPCR.

(B) hnRNPK protein expression in primary CRC and CRC liver metastasis were determined by IHC.

(C) The mRNA and protein levels of hnRNPK in CRC cells and normal cells (HCoEpiC) were detected by RT-qPCR and western blotting.

(D) The interference and overexpression efficiency of hnRNPK were examined by RT-qPCR and western blotting in HCT116 cells transfected with shCtrl/sh-hnRNPK and HT-29 cells transfected with Vector/hnRNPK.

(E) The mRNA and protein expression levels of hnRNPK were determined by RT-qPCR and western blotting in HCT116 and HT-29 cells treated with SHP2^{WT}, SHP2^{D61Y}, and SHP2^{E76K}.

Figure 8. *Continued*

(F) HCT116 cells were transfected or co-transfected with shNC, sh-PKM2, sh-PKM2SHP2^{WT}, sh-PKM2+SHP2^{D61Y}, sh-PKM2+SHP2^{E76K}; whereas HT-29 were transfected or co-transfected with Vector, PKM2, PKM2+SHP2^{WT}, PKM2+SHP2^{D61Y}, PKM2+SHP2^{E76K}. The mRNA and protein expression levels of hnRNPK were determined by RT-qPCR and western blotting.

(G–I) HCT116 cells were transfected or co-transfected with shCtrl, sh-hnRNPK, sh-hnRNPK+SHP2^{WT}, sh-hnRNPK+SHP2^{D61Y}, sh-hnRNPK +SHP2^{E76K}; whereas HT-29 were transfected or co-transfected with Vector, hnRNPK, +SHP2^{WT}, hnRNPK+SHP2^{D61Y}, hnRNPK+SHP2^{E76K}.

(G) Cell proliferation abilities were examined by CCK-8 assays in HCT116 and HT-29 cells as described previously.

(H and I) Glucose uptake and lactate production were assessed in HCT116 and HT-29 cells as described previously.

(J and K) ECAR analysis was conducted in HCT116 and HT-29 cells by Seahorse XF assays as described previously.

(L) The protein expression level of key glycolytic enzymes was determined by western blotting in HCT116 and HT-29 cells as described previously. *$p < 0.05$, **$p < 0.01$, and ***$p < 0.001$.

SUPPLEMENTAL INFORMATION

Supplemental information can be found online at https://doi.org/10.1016/j.isci.2024.110462.

ACKNOWLEDGMENTS

This study was sponsored by the Shanghai Clinical Research Center for Interventional Medicine (19MC1910300), Fudan Zhongshan Clinical Research Fund (ZSBY022) and Beijing Medical Award Fund Hengrui medical research programme (YXJL 2022-0972-1225).

AUTHOR CONTRIBUTIONS

B.Z., Z.F., and G.H: methodology; data curation; formal analysis; investigation; validation; writing—original draft. W.Z.: resources; software; methodology; data curation; validation. G.Y.: methodology; data curation; validation. L.Y., J.X., and R.L.: conceptualization; funding acquisition; project administration; supervision; writing—review & editing.

DECLARATION OF INTERESTS

The authors declare no conflict of interest.

Received: December 19, 2023
Revised: April 14, 2024
Accepted: July 2, 2024
Published: July 6, 2024

REFERENCES

1. Biller, L.H., and Schrag, D. (2021). Diagnosis and Treatment of Metastatic Colorectal Cancer: A Review. JAMA *325*, 669–685.
2. Ciardiello, F., Ciardiello, D., Martini, G., Napolitano, S., Tabernero, J., and Cervantes, A. (2022). Clinical management of metastatic colorectal cancer in the era of precision medicine. CA. Cancer J. Clin. *72*, 372–401.
3. Baidoun, F., Elshiwy, K., Elkeraie, Y., Merjaneh, Z., Khoudari, G., Sarmini, M.T., Gad, M., Al-Husseini, M., and Saad, A. (2021). Colorectal Cancer Epidemiology: Recent Trends and Impact on Outcomes. Curr. Drug Targets *22*, 998–1009.
4. Li, J., Ma, X., Chakravarti, D., Shalapour, S., and DePinho, R.A. (2021). Genetic and biological hallmarks of colorectal cancer. Genes Dev. *35*, 787–820.
5. Huang, D., Sun, W., Zhou, Y., Li, P., Chen, F., Chen, H., Xia, D., Xu, E., Lai, M., Wu, Y., and Zhang, H. (2018). Mutations of key driver genes in colorectal cancer progression and metastasis. Cancer Metastasis Rev. *37*, 173–187.
6. Yu, S., Zang, W., Qiu, Y., Liao, L., and Zheng, X. (2022). Deubiquitinase OTUB2 exacerbates the progression of colorectal cancer by promoting PKM2 activity and glycolysis. Oncogene *41*, 46–56.
7. Chen, J., Zhang, Z., Ni, J., Sun, J., Ju, F., Wang, Z., Wang, L., and Xue, M. (2022). ENO3 promotes colorectal cancer progression by enhancing cell glycolysis. Med. Oncol. *39*, 80.
8. Wong, T.L., Ng, K.Y., Tan, K.V., Chan, L.H., Zhou, L., Che, N., Hoo, R.L.C., Lee, T.K., Richard, S., Lo, C.M., et al. (2020). CRAF Methylation by PRMT6 Regulates Aerobic Glycolysis-Driven Hepatocarcinogenesis via ERK-Dependent PKM2 Nuclear Relocalization and Activation. Hepatology *71*, 1279–1296.
9. Zhao, J., Li, J., Hassan, W., Xu, D., Wang, X., and Huang, Z. (2020). Sam68 promotes aerobic glycolysis in colorectal cancer by regulating PKM2 alternative splicing. Ann. Transl. Med. *8*, 459.
10. Zhao, G., Yuan, H., Li, Q., Zhang, J., Guo, Y., Feng, T., Gu, R., Ou, D., Li, S., Li, K., and Lin, P. (2022). DDX39B drives colorectal cancer progression by promoting the stability and nuclear translocation of PKM2. Signal Transduct. Targeted Ther. *7*, 275.
11. Yang, W., Xia, Y., Ji, H., Zheng, Y., Liang, J., Huang, W., Gao, X., Aldape, K., and Lu, Z.

(2011). Nuclear PKM2 regulates beta-catenin transactivation upon EGFR activation. Nature *480*, 118–122.

12. Zhu, L., Tian, Q., Gao, H., Wu, K., Wang, B., Ge, G., Jiang, S., Wang, K., Zhou, C., He, J., et al. (2022). PROX1 promotes breast cancer invasion and metastasis through WNT/β-catenin pathway via interacting with hnRNPK. Int. J. Biol. Sci. *18*, 2032–2046.
13. Wu, H., Du, J., Li, C., Li, H., Guo, H., and Li, Z. (2022). Kaempferol Can Reverse the 5-Fu Resistance of Colorectal Cancer Cells by Inhibiting PKM2-Mediated Glycolysis. Int. J. Mol. Sci. *23*, 3544.
14. Wang, J., Sun, M., Ma, R., Wang, G., Li, W., Yang, B., and Yang, Y. (2022). Down-regulation of NOTCH1 and PKM2 can inhibit the growth and metastasis of colorectal cancer cells. Am. J. Transl. Res. *14*, 5455–5465.
15. Dong, L., Han, D., Meng, X., Xu, M., Zheng, C., and Xia, Q. (2021). Activating Mutation of SHP2 Establishes a Tumorigenic Phonotype Through Cell-Autonomous and Non-Cell-Autonomous Mechanisms. Front. Cell Dev. Biol. *9*, 630712.
16. Zhang, J., Zhang, F., and Niu, R. (2015). Functions of Shp2 in cancer. J. Cell Mol. Med. *19*, 2075–2083.
17. Zhang, Q., Li, Y., Zhao, R., Wang, X., Fan, C., Xu, Y., Liu, Y., Li, J., and Wang, S. (2018). The gain-of-function mutation E76K in SHP2 promotes CAC tumorigenesis and induces EMT via the Wnt/β-catenin signaling pathway. Mol. Carcinog. *57*, 619–628.
18. Yang, W., Zheng, Y., Xia, Y., Ji, H., Chen, X., Guo, F., Lyssiotis, C.A., Aldape, K., Cantley, L.C., and Lu, Z. (2012). ERK1/2-dependent phosphorylation and nuclear translocation of PKM2 promotes the Warburg effect. Nat. Cell Biol. *14*, 1295–1304.
19. Zhang, Z., Zhou, C., Chang, Y., Zhang, Z., Hu, Y., Zhang, F., Lu, Y., Zheng, L., Zhang, W., Li, X., and Li, X. (2016). Long non-coding RNA CASC11 interacts with hnRNP-K and activates the WNT/β-catenin pathway to promote growth and metastasis in colorectal cancer. Cancer Lett. *376*, 62–73.
20. Mucha, B., Qie, S., Bajpai, S., Tarallo, V., Diehl, J.N., Tedeschi, F., Zhou, G., Gao, Z., Flashner, S., Klein-Szanto, A.J., et al. (2022). Tumor suppressor mediated ubiquitylation of hnRNPK is a barrier to oncogenic translation. Nat. Commun. *13*, 6614.
21. Peng, C., Tan, Y., Yang, P., Jin, K., Zhang, C., Peng, W., Wang, L., Zhou, J., Chen, R., Wang, T., et al. (2021). Circ-GALNT16 restrains colorectal cancer progression by enhancing the SUMOylation of hnRNPK. J. Exp. Clin. Cancer Res. *40*, 272.
22. Good, A.L., Haemmerle, M.W., Oguh, A.U., Doliba, N.M., and Stoffers, D.A. (2019). Metabolic stress activates an ERK/hnRNPK/DDX3X pathway in pancreatic β cells. Mol. Metabol. *26*, 45–56.
23. Nguyen, L.H., Goel, A., and Chung, D.C. (2020). Pathways of Colorectal Carcinogenesis. Gastroenterology *158*, 291–302.
24. Fang, Y., Shen, Z.Y., Zhan, Y.Z., Feng, X.C., Chen, K.L., Li, Y.S., Deng, H.J., Pan, S.M., Wu, D.H., and Ding, Y. (2019). CD36 inhibits beta-catenin/c-myc-mediated glycolysis through ubiquitination of GPC4 to repress colorectal tumorigenesis. Nat. Commun. *10*, 3981.
25. Jing, Z., Liu, Q., He, X., Jia, Z., Xu, Z., Yang, B., and Liu, P. (2022). NCAPD3 enhances Warburg effect through c-myc and E2F1 and promotes the occurrence and progression of colorectal cancer. J. Exp. Clin. Cancer Res. *41*, 198.
26. Wang, Y., Pan, S., He, X., Wang, Y., Huang, H., Chen, J., Zhang, Y., Zhang, Z., and Qin, X. (2021). CPNE1 Enhances Colorectal Cancer Cell Growth, Glycolysis, and Drug Resistance Through Regulating the AKT-GLUT1/HK2 Pathway. OncoTargets Ther. *14*, 699–710.
27. Tang, C., Luo, H., Luo, D., Yang, H., and Zhou, X. (2018). Src homology phosphotyrosyl phosphatase 2 mediates cisplatin-related drug resistance by inhibiting apoptosis and activating the Ras/PI3K/Akt1/survivin pathway in lung cancer cells. Oncol. Rep. *39*, 611–618.
28. Zheng, H., Yu, W.M., Waclaw, R.R., Kontaridis, M.I., Neel, B.G., and Qu, C.K. (2018). Gain-of-function mutations in the gene encoding the tyrosine phosphatase SHP_2 induce hydrocephalus in a catalytically dependent manner. Sci. Signal. *11*, eaao1591.
29. Li, W.Y., Wei, H.Y., Sun, Y.Z., Zhou, H., Ma, Y., and Wang, R.L. (2018). Exploring the effect of E76K mutation on SHP2 cause gain-of-function activity by a molecular dynamics study. J. Cell. Biochem. *119*, 9941–9956.
30. LaRochelle, J.R., Fodor, M., Vemulapalli, V., Mohseni, M., Wang, P., Stams, T., LaMarche, M.J., Chopra, R., Acker, M.G., and Blacklow, S.C. (2018). Structural reorganization of SHP2 by oncogenic mutations and implications for oncoprotein resistance to allosteric inhibition. Nat. Commun. *9*, 4508.
31. Tien, S.C., and Chang, Z.F. (2014). Oncogenic Shp2 disturbs microtubule regulation to cause HDAC6-dependent ERK hyperactivation. Oncogene *33*, 2938–2946.
32. Wu, T.R., Hong, Y.K., Wang, X.D., Ling, M.Y., Dragoi, A.M., Chung, A.S., Campbell, A.G., Han, Z.Y., Feng, G.S., and Chin, Y.E. (2002). SHP-2 is a dual-specificity phosphatase involved in Stat1 dephosphorylation at both tyrosine and serine residues in nuclei. J. Biol. Chem. *277*, 47572–47580.
33. Ivins Zito, C., Kontaridis, M.I., Fornaro, M., Feng, G.S., and Bennett, A.M. (2004). SHP-2 regulates the phosphatidylinositide 3′-kinase/Akt pathway and suppresses caspase 3-mediated apoptosis. J. Cell. Physiol. *199*, 227–236.
34. Liu, M., Gao, S., Elhassan, R.M., Hou, X., and Fang, H. (2021). Strategies to overcome drug resistance using SHP2 inhibitors. Acta Pharm. Sin. B *11*, 3908–3924.
35. Yuan, X., Bu, H., Zhou, J., Yang, C.Y., and Zhang, H. (2020). Recent Advances of SHP2 Inhibitors in Cancer Therapy: Current Development and Clinical Application. J. Med. Chem. *63*, 11368–11396.
36. Shen, D., Chen, W., Zhu, J., Wu, G., Shen, R., Xi, M., and Sun, H. (2020). Therapeutic potential of targeting SHP2 in human developmental disorders and cancers. Eur. J. Med. Chem. *190*, 112117.
37. Nabinger, S.C., and Chan, R.J. (2012). Shp2 function in hematopoietic stem cell biology and leukemogenesis. Curr. Opin. Hematol. *19*, 273–279.
38. Fan, Y., Hou, T., Dan, W., Zhu, Y., Liu, B., Wei, Y., Wang, Z., Gao, Y., Zeng, J., and Li, L. (2022). ERK1/2 inhibits Cullin 3/SPOP-mediated PrLZ ubiquitination and degradation to modulate prostate cancer progression. Cell Death Differ. *29*, 1611–1624.
39. Wu, H.L., Li, S.M., Huang, Y.C., Xia, Q.D., Zhou, P., Li, X.M., Yu, X., Wang, S.G., Ye, Z.Q., and Hu, J. (2021). Transcriptional regulation and ubiquitination-dependent regulation of HnRNPK oncogenic function in prostate tumorigenesis. Cancer Cell Int. *21*, 641.
40. Zhou, Q., Yin, Y., Yu, M., Gao, D., Sun, J., Yang, Z., Weng, J., Chen, W., Atyah, M., Shen, Y., et al. (2022). GTPBP4 promotes hepatocellular carcinoma progression and metastasis via the PKM2 dependent glucose metabolism. Redox Biol. *56*, 102458.
41. Zhang, W., Zhang, X., Huang, S., Chen, J., Ding, P., Wang, Q., Li, L., Lv, X., Li, L., Zhang, P., et al. (2021). FOXM1D potentiates PKM2-mediated tumor glycolysis and angiogenesis. Mol. Oncol. *15*, 1466–1485.
42. Xu, Y., Wu, W., Han, Q., Wang, Y., Li, C., Zhang, P., and Xu, H. (2019). Post-translational modification control of RNA-binding protein hnRNPK function. Open Biol. *9*, 180239.

STAR★METHODS

KEY RESOURCES TABLE

REAGENT or RESOURCE	SOURCE	IDENTIFIER
Antibodies		
SHP2	Abcam	RRID: AB_300579
Bcl-2	Abcam	RRID: AB_196495
Bax	Abcam	RRID: AB_32503
p21	Abcam	RRID: AB_109520
E2F1	Abcam	RRID: AB_4070
PKM2	Abcam	RRID: AB_150377
ERK1/2	Abcam	RRID: AB_184699
LDHA	Abcam	RRID: AB_52488
LDHB	Abcam	RRID: AB_240482
HK-2	Abcam	RRID: AB_209847
hnRNPK	Abcam	RRID: AB_52600
β-actin	Abcam	RRID: AB_20272
GAPDH	Abcam	RRIS: AB_8245
Lamin B1	Abcam	RRID: AB_16048
Biological samples		
Human CRC tissues	Zhongshan Hospital, Fudan University	This paper
Chemicals, peptides, and recombinant proteins		
DAPI	Millipore, Billerica, MA	Cat#28718-90-3
Cisplatin	Millipore, Billerica, MA	Cat#15663-27-1
LipofectamineTM 2000	Thermo Fisher Scientific	Cat# 11668019
Dulbecco Modified Eagle Medium	Thermo Fisher Scientific	Cat# C11965500BT
Penicillin-streptomycin	Thermo Fisher Scientific	Cat# 15140122
XF assay medium	Seahorse	Cat#103576-100
2-deoxyglucose	MCE	Cat# HY-13966
oligomycin	MCE	Cat# HY-125335
glucose	MCE	Cat#HY156518
Hematoxylin	Beyotime	Cat#C0105M
TUNEL	MCE	Cat#HY-K1091
RIPA lysis buffer	Thermo Fisher Scientific	Cat# 89900
BCA Protein assay kit	Thermo Fisher Scientific	Cat#23225
IP lysis buffer	Thermo Fisher Scientific	Cat# 87787
polyvinylidene fluoride (PVDF) membranes	Millipore, Billerica, MA	Cat#GVWP02500
4% paraformaldehyde	MCE	Cat# HY-Y0333
Fetal bovine serum	Thermo Fisher Scientific	Cat# 10270-106
Critical commercial assays		
XFp Extracellular Flux Analyzer	Seahorse Bioscience	N/A
a light microscope	Leica DM IL, Germany	N/A
FITC Annexin V Apoptosis Detection Kit	BD Biosciences, San Jose,	#556547
Glucose Uptake Fluorometric Assay Kits	Biovision, Milpitas, CA	#K666-100
Lactate Colorimetric Assay Kits	Biovision, Milpitas, CA	#K627-100
cell counting kit-8	Dojindo, Kumamoto	#SKU: CK04

(*Continued on next page*)

Continued

REAGENT or RESOURCE	SOURCE	IDENTIFIER
Experimental models: Cell lines		
HT-29	HyClone	N/A
SW480	HyClone	N/A
VACO432	HyClone	N/A
HCT116	HyClone	N/A
HCoEpiC	HyClone	N/A
Experimental models: Organisms/strains		
BALB/c nude mice	Shanghai Slack Laboratory Animal Co. Ltd	N/A
Oligonucleotides		
Primers used for qRT-PCR, see Table S2.	This paper	N/A
Software and algorithms		
GraphPad Prism 8.0	GraphPad	N/A
FACSVerse flow cytometry system	BD Biosciences	N/A
ImageJ software	National Institutes of Health	N/A

RESOURCE AVAILABILITY

Lead contact

Further information request for resources and reagents should be directed to and will be fulfilled by the lead contract, Rong Liu (liu.rong@zs-hospital.sh.cn).

Materials availability

This study did not generate new unique reagents.

Data and code availability

- Date: Data reported in this paper will be shared by the lead contact upon request.
- Code: This paper does not report original code.
- All other requests: Any additional information required to reanalyze the data reported will be shared by the lead contact upon request.

EXPERIMENTAL MODEL AND STUDY PARTICIPANT DETAILS

Ethics approval and consent to participate

All procedures performed in studies involving human participants were in accordance with the ethical standards of Zhongshan Hospital, Fudan University. Informed consents were obtained from all individual participants included in the study. Animal experiments were approved by the Experimental Animal Care Commission of Zhongshan Hospital, Fudan University.

Human materials

Tumors and adjacent tissues were collected from 47 patients with CRC who attended Zhongshan Hospital, Fudan University. The patients had provided written consent and the study was approved by the Research Ethics Committee of the Zhongshan Hospital, Fudan University (Shanghai, China). The patient's information with gene mutations were listed in the Tables S3A, S3B, S3C, S3D, S3E, S3F, and S3G.

Animals

For the *in vivo* liver metastasis model, 5-week-old female BALB/c nude mice were purchased from Shanghai Slack Laboratory Animal Co. Ltd.

METHOD DETAILS

Clinical samples

Tumors and adjacent tissues were collected from 47 patients with CRC who attended Zhongshan Hospital, Fudan University. The patients had provided written consent and the study was approved by the Research Ethics Committee of the Zhongshan Hospital, Fudan University (Shanghai, China). The patient's information with gene mutations were listed in the Table S3.

Cell culture and transfection

CRC cell lines HT-29, SW480, VACO432, and HCT116 and normal cells HCoEpiC were obtained from HyClone (Logan, UT, USA) and cultured in Dulbecco's modified Eagle's medium supplemented with 10% fetal bovine serum at 37°C in 5% CO_2. Lentiviruses expressing $SHP2^{D61Y}$, $SHP2^{E76K}$, and $SHP2^{WT}$ or corresponding controls were generated by GenePharma (Shanghai, China) and transfected into cells using Lipofectamine 2000 (Invitrogen, Carlsbad, CA, USA) following manufacturer's instructions.

Quantitative RT-PCR

Total RNA was extracted using a RNeasy Mini Kit (Qiagen, Valencia, CA, USA) according to the manufacturer's protocol. RNA was reverse-transcribed using a cDNA Synthesis Kit (Bio-Rad, Hercules, CA, USA). Real-time PCR was performed with an SYBR Green Master Mix (Invitrogen, Carlsbad, CA, USA) and the primers are listed in Table S2. Expression was determined relative to β-actin or GAPDH by using the $2^{-\Delta\Delta CT}$ method.

Western blot analysis

Proteins were extracted from cells by using RIPA lysis buffer (Thermo Fisher Scientific, Waltham, MA, USA). Levels of protein in the extracts were measured using a BCA Protein assay kit (Thermo Fisher Scientific). Equal quantities of proteins were separated with SDS-PAGE and transferred to polyvinylidene fluoride (PVDF) membranes (Millipore, Billerica, MA, USA). Membranes were blocked with 5% non-fat milk and then incubated overnight at 4°C with appropriate primary antibodies: SHP2 (Abcam, ab300579, 1:1,000), Bcl-2 (Abcam, ab196495, 1:2,000), Bax (Abcam, ab32503, 1:5,000), p21 (Abcam, ab109520, 1:2,000), E2F1 (Abcam, ab4070, 1:500), PKM2 (Abcam, ab150377, 1:2,000), ERK1/2 (Abcam, ab184699, 1:5,000), LDHA (Abcam, ab52488, 1:5,000), LDHB (Abcam, ab240482, 1:1,000), HK-2 (Abcam, ab209847, 1:1,000), hnRNPK (Abcam, ab52600, 1:10,000), β-actin (Abcam, ab20272, 1:5,000), GAPDH (Abcam, ab8245, 1:1,000), and Lamin B1(Abcam, ab16048, 1:1,000). Samples were then incubated with horseradish peroxidase secondary antibody and visualized using an ECL detection system (Bio-Rad). Protein levels were quantified with ImageJ software.

Cell counting assay

Cells from different growth conditions were plated in 96-well plates (1×10^4 cells/well). Cell proliferation was determined using cell counting kit-8 (CCK-8; #SKU: CK04, Dojindo, Kumamoto, Japan) and measured using a microplate reader according to the manufacturer's instructions.

Colony formation

Colony formation was measured in transfected HCT116 and HT-29 cells. Cells were plated onto six-well plates (500 cells/well) and cultured under experimental conditions. After incubation, cells were fixed with paraformaldehyde for 20 min and then stained with 0.5% crystal violet for 30 min. Colonies were then counted.

Glucose consumption and lactate production measurements

Cells were cultured at 37°C and 5% CO_2 for 48 h in six-well plates (3×10^5 per well). Glycolysis was detected in HCT116 and HT-29 cells by using Glucose Uptake Fluorometric Assay Kits (#K666-100, Biovision, Milpitas, CA, USA) and Lactate Colorimetric Assay Kits (#K627-100, Biovision) according to the manufacturer's protocols.

Apoptosis assay

Cells (1×10^6) were digested with 0.25% trypsin. Annexin V-FITC and propidium iodide (PI) were added successively and incubated in the dark at room temperature for 5 min according to the instructions of a FITC Annexin V Apoptosis Detection Kit (BD Biosciences, San Jose, CA, USA). Apoptotic cells were then detected using a FACSVerse flow cytometry system (BD Biosciences).

Transwell assays

Cell invasion assays were performed using a 24-well Transwell chamber (BD, Biosciences). At 48 hours after transfection, HCT116 and HT-29 cells were trypsinized and transferred to an upper chamber coated in Matrigel (BD, Biosciences) containing 100 μl of serum-free medium. FBS was added to the lower chamber as a chemoattractant. After 24 h, cells on the bottom of the chambers were fixed in 4% paraformaldehyde and stained with 0.1% crystal violet. Cells that invaded the lower surface were counted in at least five random fields (magnification: ×200, Nikon). Each experiment was performed in triplicate.

Immunofluorescence staining

Cells were initially fixed using 4% paraformaldehyde for 15 minutes at room temperature (RT). After washing samples were blocked using 10% goat serum for 20 minutes at RT. Cells were then incubated with primary antibodies against PKM2 overnight at 4°C. Cells were thoroughly washed and incubated in respective secondary antibodies (Santa Cruz Biotechnology) for 1h at RT. Finally, the cells were stained with nuclear stain DAPI for 10 minutes before visualization using a light microscope (Leica DM IL, Germany).

Seahorse assays

Extracellular acidification rate (ECAR) in HCT116 and HT-29 cell lines were determined using a Seahorse Bioscience XFe24 Extracellular Flux Analyzer (Agilent, Santa Clara, CA, USA). Cells (7.5×10^4) were seeded into Seahorse XFe24 microplates 24 h before the assay. Cells were then incubated for 1 h at 37°C with glucose (100 mM), oligomycin (10 μM), and 2-deoxy-glucose (2DG, 1M). ECAR and OCR levels were then measured to determine glycolytic capacity.

In vivo animal experiments

For the *in vivo* liver metastasis model, 5-week-old female BALB/c nude mice were purchased from Shanghai Slack Laboratory Animal Co. Ltd. For xenograft experiments, HCT116 cells transfected with control or $SHP2^{WT}$, $SHP2^{D61Y}$, and $SHP2^{E76K}$ were suspended in PBS at a concentration of 2×10^6 cells/mL, and then 50 μl of the HCT116 cell suspension was orthotopically microinjected into the tail region of the spleen. For metastasis experiments, HT-29 cells transfected with control or $SHP2^{WT}$, $SHP2^{D61Y}$, and $SHP2^{E76K}$ were suspended in PBS at a concentration of 2×10^6 cells/mL, and then 50 μl of the HT-29 cell suspension was orthotopically microinjected into the tail region of the spleen. A week later, CDDP (5 mg/kg) was injected intraperitoneally into the mice three times per week. The body weights of the nude mice were measured and tumor volumes were calculated using the formula length × $width^2/2$ every week following the injection. Five weeks after the injection, all mice were euthanized and the livers were excised to assess metastasis. For histological assessment, the samples were either stained with H&E to reveal the degree of pathological differentiation and metastatic lesions or analyzed by immunohistochemical staining. TUNEL assay was performed on the paraffin-embedded tissue sections according to the manufacturer's instructions (Promega, Madison, WI, USA). The apoptotic index was determined from the percentage of TUNEL-positive cells.

QUANTIFICATION AND STATISTICAL ANALYSIS

All data were analyzed using GraphPad Prism 8.0 (GraphPad Software Inc., La Jolla, CA, USA) and presented as the mean ± SEM. Statistical differences between two groups were determined using the Student's *t*-test. A one-way analysis of variance was used to compare multiple groups. Kaplan-Meier curves were used to determine OS. $P < 0.05$ was considered significant.